

Can bed load transport drive varying depositional behaviour in river delta environments?

Vegt, H. van der; Storms, J.E.A.; Walstra, D.J.R.; Howes, N.C.

DOI

[10.1016/j.sedgeo.2016.08.009](https://doi.org/10.1016/j.sedgeo.2016.08.009)

Publication date

2016

Document Version

Accepted author manuscript

Published in

Sedimentary Geology

Citation (APA)

Vegt, H. V. D., Storms, J. E. A., Walstra, D. J. R., & Howes, N. C. (2016). Can bed load transport drive varying depositional behaviour in river delta environments? *Sedimentary Geology*, 345, 19 - 32.
<https://doi.org/10.1016/j.sedgeo.2016.08.009>

Important note

To cite this publication, please use the final published version (if applicable).
Please check the document version above.

Copyright

Other than for strictly personal use, it is not permitted to download, forward or distribute the text or part of it, without the consent of the author(s) and/or copyright holder(s), unless the work is under an open content license such as Creative Commons.

Takedown policy

Please contact us and provide details if you believe this document breaches copyrights.
We will remove access to the work immediately and investigate your claim.

1 **Can bed load transport drive varying depositional behaviour**

2 **in river delta environments?**

3 H. van der Vegt^{*} ^a, J. E. A. Storms^a, D. J. R. Walstra^{a,b}, N. C. Howes^c

4 ^aDelft University of Technology, Mekelweg 2, 2628 CD Delft, The Netherlands

5 ^bDeltares, Boussinesweg 1, 2629 HV Delft, The Netherlands

6 ^cShell Projects and Technology, 3333 Highway 6 South, Houston, Texas 77082, U.S.A.

7

8 **Abstract**

9 Understanding the processes and conditions at the time of deposition is key to the
10 development of robust geological models which adequately approximate the
11 heterogeneous delta morphology and stratigraphy they represent. We show how the
12 mechanism of sediment transport (the proportion of the sediment supply transported
13 as bed load vs. suspended load) impacts channel kinematics, delta morphology and
14 stratigraphy, to at least the same extent as the proportion of cohesive sediment
15 supply. This finding is derived from 15 synthetic delta analogues generated by
16 processes-based simulations in Delft3D. The model parameter space varies sediment
17 transport mechanism against proportions of cohesive sediment whilst keeping the total
18 sediment mass input constant. Proximal morphology and kinematics previously
19 associated with sediment cohesivity are also produced by decreasing the proportion of
20 bed load sediment transport. However, distal depositional patterns are different for
21 changes in sediment transport and sediment load cohesivity. Changes in sediment
22 transport mechanisms are also shown to impact clinoform geometry as well as the
23 spatiotemporal scale of autogenic reorganisation through channel avulsions. We

^{*} corresponding author email: h.vandervegt@tudelft.nl

24 conclude that improving insight into the ratio of bed load to suspended load is crucial
25 to predicting the geometric evolution of a delta.

26 **Keywords**

27 River delta; Sediment transport; Bed load; Suspended load; Cohesive; Process-based
28 modelling

29 **1 Introduction**

30 Understanding deposition in deltaic environments is not only important to predict the
31 effect of anthropogenic changes in these densely populated areas (Syvitski and Saito,
32 2007), but also forms the basis of geological models of ancient deltaic deposits. The
33 heterogeneous nature of river delta morphology and stratigraphy complicates the
34 development of geological models (Howell et al., 2008). To simplify this process, a
35 number of classification schemes have been developed based on modern deltaic
36 systems. Initially, classification only characterised deltas by the hydrodynamic forces
37 acting on the system (e.g., fluvial input, tidal conditions, wave activity) (Galloway,
38 1975). Subsequently it was shown that the physical properties of the supplied
39 sediment (e.g., cohesivity, grain size) can be equally important (Orton and Reading,
40 1993; Hoyal and Sheets, 2009). Past studies have shown that the balance between
41 cohesive and non-cohesive sediments can have significant effects on deltaic
42 morphology (Peakall et al., 2007; Edmonds and Slingerland, 2009; Hoyal and Sheets,
43 2009; Geleynse et al., 2011).

44 Comparatively less attention has been given to the effects that sediment transport
45 mechanisms have on deltaic morphology and stratigraphy. Deltaic stratigraphy can be
46 viewed as a record of the sediments preserved by this evolving morphology. Sediment
47 transport ultimately regulates where and how sediment is deposited, based on local

48 hydrodynamic conditions and sediment properties. Sediment transport to and within a
49 delta environment can be simplified to two mechanisms: bed load and suspended
50 load. In deltaic systems, the majority of sediment supply is typically cohesive and
51 transported in suspension, forming the bulk of the suspended load. A smaller
52 proportion of sediment consists of non-cohesive material (sands) transported partially
53 in suspension and partially through creep and saltation, constituting the bed load.

54 Field measurements of the suspended load (the cohesive and non-cohesive sediment
55 transported in suspension) is relatively simple and can even be partially automated.
56 Bed load measurements are more expensive and labour intensive to obtain (Turowski
57 et al., 2010), especially in coastal settings. River deltas are formed at the interface
58 between the fluvial and the coastal domain and are therefore both influenced by fluvial
59 processes as well as marine reworking. Existing work primarily considers fluvial
60 systems with some work having been conducted at coastlines (van Rijn, 2007). In
61 experimental settings of such systems, there are various challenges associated with
62 the scaling of sediment transport (Paola et al., 2009).

63 Due to the limited data availability, bed load is typically estimated or calculated based
64 on the suspended load measurements (e.g., Syvitski and Saito, 2007, Kleinhans et al.,
65 2012). Turowski et al. (2010) conducted an extensive review of reported values for bed
66 load, but found that often no reference is made to original data. They traced the source
67 of most data back to a data table in a report from the 1950's (Maddock and Borland,
68 1950) which claimed to "give data on estimates of the unmeasured bed load of
69 streams based on the Bureau of Reclamation experience". Available measurements
70 are mainly for fluvial systems, which Turowski et al. (2010) compiled in their review. It
71 shows that between 1% and 50% of the total sediment load can be transported as bed

72 load. For ephemeral rivers, however, the percentage can be even higher, up to 100%
73 (Turowski et al., 2010, Karimae Tabarestani and Zarrati, 2015).

74 Various factors have been hypothesised to influence the balance between suspended
75 load and bed load transport in fluvial systems. Locally this balance is determined by
76 particle size, weight, shape and hydraulic conditions, while on a larger scale
77 influencing factors may include catchment geology, climate and relief (Laronne and
78 Reid, 1993; Kleinhans and Grasmeijer, 2006; van Rijn, 2007; Turowski et al., 2010;
79 Karimae Tabarestani and Zarrati, 2015). Turowski et al. (2010) conclude that there is
80 not yet sufficient data available to isolate the effect of different parameters on the
81 partitioning between sediment transported as bed load and suspended load.

82 Even with this limited data availability, previous studies of river morphologies have
83 identified the proportion of sediment supply transported as bed load as an important
84 control on sediment depositional patterns (Kleinhans, 2010; Turowski et al., 2010;
85 Ashworth and Lewin, 2012). Considering the challenges associated with gathering
86 field data of bed load transport, it is imperative to better understand the implications of
87 these processes on delta morphology and stratigraphy prior to undertaking field
88 studies. In addition, field studies are limited by the availability of appropriate data or
89 field sites and often cannot span the entire parameter space of interest. Comparing
90 different natural systems involves variations in many parameters at the same time.
91 Conducting a modelling study allows the detailed investigation of individual processes
92 and in so doing extend and supplement experimental and field-based studies.

93 In this study we examine the effect of both sediment transport mechanism and
94 cohesive sediment content on depositional geometries in fluvial dominated deltas. We
95 propose that the mechanism of sediment transport (i.e., what proportion of the

96 sediment supply is transported as bed load vs. suspended load) impacts depositional
97 behaviour to at least the same extent as sediment properties, such as cohesivity.

98 In this study we use process-based simulations to assess the effects of sediment
99 transport mechanism compared to sediment composition on deltaic morphology and
100 stratigraphy. As predictions made with process-based models are consistent, and they
101 allow careful control of boundary conditions, the quantitative output can be compared,
102 and specific processes or mechanisms can be isolated. Following this approach we
103 explore three metrics: (1) channel geometry and channel dynamics, (2) locations of
104 sediment deposition, reworking and preservation, and (3) large scale delta geometry.
105 We also discuss the relationships between these quantitative measures. The metrics
106 developed here can be applied to other fluvio-deltaic model ensembles to study the
107 implications of a range of boundary conditions on delta morphology and stratigraphy.

108 **2 Experimental design**

109 We created an ensemble of 15 numerical models using the open source process-
110 based modelling software Delft3D (Lesser et al., 2004). Models were calculated using
111 Delft3D Flow (Version 4168) with parallel processing on a single, Linux operating, 16-
112 core node. For detailed descriptions of the governing equations representing each of
113 the processes as well as the finite difference solution methodology the reader is
114 referred to the Delft3D-Flow documentation which is freely available online. In past
115 studies, Delft3D has been extensively applied to study the effects of hydrodynamic
116 forcing and sediment properties on river delta morphodynamics (e.g., Edmonds and
117 Slingerland, 2009; Geleynse et al., 2010, 2011; 2012; Caldwell and Edmonds, 2014).
118 Our numerical experiments investigate the implications of mechanism of sediment
119 transport on depositional behaviour in a river delta.

120 **2.1 Bathymetry, hydrodynamic forcing and sediment properties**

121 Parameters described in this section were applied to all 15 experiments. The starting
122 bathymetry is similar to that described in previous studies, consisting of a channel
123 delivering water and sediment into a sloped basin already filled with fresh water
124 (Geleynse et al., 2011). One change is that our channel is partially formed by two
125 floodplains sloping toward the basin and channel. This forms a trumpet-shaped
126 channel debouching into the basin, representative of a river mouth towards the end of
127 a rising sea-level cycle. However, sea level was kept constant during the model runs.
128 The initial channel width is 1000 m and with constant discharge of $1500 \text{ m}^3 \text{ s}^{-1}$. This
129 discharge should be considered as a continuous bankfull flood stage. A tide with
130 amplitude of 1 m was added to introduce dynamics into an otherwise very steady
131 system. The effect of flocculation was not considered in this study.

132 The total sediment supply was estimated based on average suspended load
133 measurements in modern delta systems of a similar scale (Milliman and Farnsworth,
134 2011). This resulted in a total load concentration of 0.2 kg m^{-3} being applied across the
135 models. The sediment transport calculations do not take migrating bedforms into
136 account, although a Manning roughness coefficient of 0.02 implicitly accounts for the
137 impact of smaller scale bedforms on hydrodynamics.

138 Calculations span a full hydrodynamic year, but include a morphological scaling factor
139 (MORFAC) of 60 (Ranasinghe et al., 2011). Combining this with continuous bankfull
140 discharge results in deposition equivalent to delta evolution on a millennial timescale.
141 Simulation output was recorded at the end of each of the 366 hydrodynamic days.

142 **2.2 Cohesivity vs. sediment transport**

143 The majority of sediment supplied to deltaic environments consists of a cohesive silt
144 and clay mixture. These sediment types are typically transported as part of the
145 suspended load. Suspended load in Delft3D is calculated by solving a depth-averaged
146 (2DH) advection-diffusion (mass-balance) equation for the suspended sediment
147 (Galappatti, 1983). The remainder of the sediment is non-cohesive (sands and
148 gravels) and is transported partially in suspension, adding to the suspended load, and
149 partially through saltation and creep, constituting the bed load.

150 Previous simulations of delta formation in Delft3D have used the default Van Rijn
151 (1993) transport formulation (van Rijn, 1993; Edmonds and Slingerland, 2009;
152 Caldwell and Edmonds, 2014) or the Engelund-Hansen transport formulation
153 (Engelund and Hansen, 1967; Geleynse et al., 2011, 2010; Guo et al., 2015) to
154 determine sediment transport of non-cohesive sediment (sands). The Engelund-
155 Hansen formulation reflects total transport. However, its implementation allows for the
156 partitioning of sands into a suspended load and a bed load fraction, for which the
157 transport is calculated separately.

158 For our simulations, we selected and implemented the Engelund-Hansen transport
159 model after a series of sensitivity studies with the available sediment transport
160 formulas in Delft3D. The total fluvial sediment input of 0.2 kg m^{-3} is made up of four
161 sediment classes, as defined in Figure 1. The properties for the individual sediment
162 classes as well as the total sediment supply concentration are the same in all
163 simulations.

164 The model parameter space explores the role of sediment transport and sediment
165 composition on delta development. The effect of sediment transport mechanism is
166 explored by varying the relative proportions of bed load versus suspended load

167 transport. The effect of bulk composition is explored by varying the cohesive versus
168 the non-cohesive sediment fraction. This is done by varying the proportions of the
169 sediments defined in Figure 1. The exact concentrations of each sediment class as
170 well as an estimated D_{50} grain size value of the sediment input is provided in Table 1.
171 Cohesive sediment fractions are defined using a settling velocity rather than a grain
172 size, therefore Stokes' Law is used to convert these values to a grain size value used
173 in the calculation of the overall D_{50} of the sediment supply. As a consequence of
174 varying the balance between cohesive and non-cohesive sediment by means of
175 adjusting the input concentrations of pre-defined sediment classes, the mean grain
176 size value also increases with increasing non-cohesive sediment supply.

177 The translation of this parameter space into the model input is visualised in Figure 2.
178 To simplify presentation and discussion of the results we have divided the model
179 parameter space in Figure 2 into quadrants. Columns are separated into models with
180 the highest suspended load supply (SL) or models with the highest bed load supply
181 (BL). Rows are divided into models with the highest cohesive sediment supply (CS) or
182 models with the highest non-cohesive sediment supply (NS). These abbreviations will
183 be referred to when comparing depositional trends relating to these differences in
184 cohesivity and sediment transport.

185 **2.3 Analysis and processing**

186 A delta is an evolving landform with morphology and stratigraphy changing over time.
187 To account for the evolution of the depositional behaviour, the analyses were
188 performed per output time interval. Output files contain a record of the bathymetry and
189 the hydrodynamic conditions prevailing at each output time step. This provides insight

190 into the morphology and stratigraphy as the delta evolves, as well as the processes
191 controlling its evolution.

192 The first set of analyses pertains to the morphology and kinematics of the channel
193 network. The channels constitute a distributed sediment supply network across the
194 delta top and delta front. In addition to acting as a sediment source, the active
195 channels are also the main erosive features responsible for reworking of sediment.

196 We defined the active channel network to consist of locations with high sediment
197 transport values together with large flow velocity or erosion. Active channel network
198 locations must have a water depth greater than 0.5 m. Owing to the element size of 50
199 m x 50 m horizontally, a water depth of less than 0.5 m would imply a width:depth ratio
200 of more than 100. This value falls well outside of the definition of a channel, filtering
201 out sheet flow at the current grid resolution (Gibling, 2006; Hajek and Wolinsky, 2012).
202 Channel depth, a proxy for the erosive properties of the network, has implications for
203 the reworking of underlying sediment. The average channel depth with respect to the
204 elevation of the surrounding delta plain/delta top was also calculated for each model at
205 every time interval.

206 The channel network does not occupy the same locations over time. As channels
207 prograde into the basin, individual channels can bifurcate, migrate laterally, avulse or
208 become abandoned (Kleinhans, 2010). All of these processes lead to new areas of the
209 delta top becoming incorporated into the active channel network while other areas no
210 longer form part of this network. We calculated the proportion of the active channel
211 network which overlaps with part of the active channel network of the previous output
212 time interval as an indication of channel network mobility. The channel overlap
213 (mobility) has implications for both for the scale of lateral reworking of sediments as

214 well as the distribution of sediment deposition across the delta network (Jerolmack and
215 Mohrig, 2007).

216 Understanding where sediment was deposited and where it was subsequently
217 reworked provides insight into the preserved stratigraphy of the delta. Deposited
218 sediment was divided into four depositional units based on location and depositional
219 processes. These consist of the following categories (Fig. 3):

220 (1) Channel deposits: Consist of accretion deposits as channels migrate or
221 aggrade as well as channel fill following an avulsion. This was defined as any
222 sediment deposited at active channel locations, or at a location that was part of the
223 active channel network until the elevation at that position equals the average elevation
224 of surrounding delta top.

225 (2) Overbank deposits: Consist of sediment deposited on the delta top outside of
226 the active channel network.

227 (3) Lobate deposits: These deposits were defined by rate of deposition, as
228 locations where more than 0.15 m of sediment was deposited in one output time
229 interval. This thickness definition is based on inspection of the results as well as the
230 vertical resolution of the grid. The lobate deposits are supplied by sediment exiting the
231 channel mouths and extend to depths of approximately 15 m to 20 m below sealevel
232 across the model parameter space.

233 (4) Distal deposits: In the case of our analysis, the distal element is a background
234 element consisting of all remaining deposits not yet accounted for within the above
235 elements.

236 For the purpose of analysis it is necessary to define a clear boundary between lobate
237 and distal deposits, however it is also important to recognise that in natural systems
238 this transition is gradual.

239 In addition to calculating the depositional units deposited, we are especially interested
240 in the reworking and preservation of these units. The preserved depositional units
241 drive the final geometry of the delta. For example, preserved channel and overbank
242 deposits drive delta top aggradation while preserved lobate deposits drive delta
243 progradation. In order to assess the changes in large scale geometric trends, we
244 calculated the average elevation as a function of distance from the delta apex. For this
245 purpose, radially averaged topographies were constructed as shown in Figure 4. The
246 model results were mapped to polar coordinates with an origin located at the delta
247 apex. This allows each location in the delta bathymetry to be described by the distance
248 from apex and angle from the original coastline. The boundaries on either side of the
249 apex were defined at 20° and 160° respectively to account for the initial trumpet
250 shaped bathymetry. At intervals of active channel elements were not included in the
251 calculation, such that the bathymetry only constitutes the delta top, delta front and
252 prodelta. The elevation was averaged across all angles from 20° to 160° and plotted
253 as a function of distance from apex at intervals of 125 m (Fig. 4B, C). For each model,
254 366 topographic profiles were constructed, representing the 366 output time intervals
255 (Fig. 4E). For each profile the location of the brink point (separating the delta top and
256 delta front) and delta toe (separating the delta front and pro delta) were identified (Fig.
257 4D).

258 **3 Results**

259 The ensemble of numerical simulations allows us to study and compare the evolving
260 geometry (morphologic and stratigraphic) and kinematics of the deltas within our
261 parameter space. Figure 5 displays a plan view of the bathymetry at the end of each of
262 the 15 simulations. Bathymetry has been corrected for local water levels. These can
263 be higher proximally due to the backwater effect.

264 In order to evaluate the depositional behaviour of an evolving landform, we need to
265 compare analyses which account for change in behaviour over time, starting with
266 channel morphology and kinematics. The active channel network acts as a distributed
267 sediment source across the delta top and, as such, drives the location of sediment
268 deposition. Additionally, the active channel network occupies different locations over
269 time, eroding lateral and underlying sediment. Hereby channel kinematics determine
270 the locations at which sediment is reworked. We separate the volume of sediment
271 which is reworked after its initial deposition, obtaining the volume of preserved
272 deposits. Deposited sediment is classified by depositional unit in order to differentiate
273 between the conditions under which the sediment was deposited. Large scale delta
274 geometry is in turn a product of these preserved depositional units.

275 **3.1 Channel morphology and kinematics**

276 In this section we focus on channel properties (morphology and kinematics) which
277 drive sediment deposition and reworking. The channel depth relative to the
278 surrounding delta top elevation was determined for each model in the ensemble. The
279 mean depth (spatially and temporally) was then calculated for each model across all
280 timesteps (Fig. 6). Channels are shallower both with less cohesive sediment supply
281 (Fig. 6, Models 1.1, 2.1, 2.3, 2.4 compared to Models 1.3, 2.4, 3.4, 4.4 respectively)

282 and less suspended load (Fig. 6, Model 1.1, 1.2, 1.3 compared to Models 4.1, 4.2, 4.3
283 respectively).

284 Mean values of channel overlap were calculated (Fig. 6) as a proxy for channel
285 mobility. Channel mobility is greater in BL- and NS-models while channel networks in
286 their corresponding SL- and CS-models tend to occupy the same locations for longer
287 periods of time.

288 **3.2 Sediment reworking and preservation**

289 During the simulation, sediment is deposited in varying quantities across the model
290 domain. At the same time, previously deposited sediment is eroded (reworked) by the
291 evolving channel network. Subtracting the reworked sediment from the total deposited
292 sediment provides the net volume of sediment deposited. This volume of net
293 deposition is reasonably constant for each output time interval. Eroded (reworked)
294 sediment can be re-deposited in one of the following time intervals and ultimately
295 preserved. The cumulative volume of preserved deposits increases over time as the
296 delta progrades and can be calculated as the cumulative net deposition.

297 The volume of reworked sediment varies significantly between simulations (Fig. 7).

298 The model where deposited sediment undergoes the most reworking (model 4.4, Fig.
299 7) shows more than 5 times as much reworking than the model experiencing the least
300 reworking (model 1.1, Fig. 7). In contrast, the volumes of preserved deposits are
301 relatively constant between simulations. The model preserving the largest volume of
302 sediment (model 1.3, Fig. 7) preserves only 1.4 times as much sediment as the model
303 preserving the least (model 4.1, Fig. 7).

304 More sediment deposited in BL-models undergo reworking than in SL-models. This is
305 illustrated by the larger blue area in models 1.3, 2.4, 3.4, and 4.4 (Fig. 7) compared to

306 models 1.1, 2.1, 3.1 and 4.1 (Fig. 7) respectively. To a lesser extent, slightly more
307 sediment deposited in NS-models undergoes reworking compared to those deposited
308 in CS-models. This is illustrated by the larger blue area in models 4.1, 4.2, 4.3 and 4.4
309 (Fig. 7) compared to models 1.1, 1.2, 1.3 and 2.4 (Fig. 7) respectively. Therefore, both
310 more bed load transport or more non-cohesive sediment leads to a greater volume of
311 sediment reworking. As the delta evolves, the volume of reworked sediment per output
312 time interval increases and the differences between the models become even more
313 pronounced. Therefore, both an increase in bed load transport and decrease in
314 sediment cohesion can drive divergent behaviour delta top reworking.

315 The total deposited sediment was classified into four depositional units: channel
316 deposits, overbank deposits, lobate deposits and distal deposits. This classification
317 was also extended to the reworked and preserved deposits. Sediment reworking
318 occurred mainly in channel and overbank deposits, which constitute the delta top, and
319 to a smaller extent in the lobate deposits which are found mainly in the delta front (Fig.
320 8). Only in shallower, proximal regions, where a thinner layer of channel, overbank and
321 lobate sediments were deposited (as a result of the sloped basin), did sediment
322 erosion reach older distal deposits or initial substrate (e.g., Fig. 3). Sediment eroded
323 from the substrate contributed less than 0.2% of the total sediment supplied to the
324 systems and was not included in the analyses.

325 SL-CS models (model 1.1, 1.2, 2.1, 2.2) show smaller volumes of delta top reworking
326 compared to BL-NS models (models 3.3, 3.4, 4.3, 4.4). SL-CS models also exhibit
327 larger proportion of lobate and distal deposit reworking. As the delta top grows over
328 time, a larger volume of channel and overbank deposits undergo reworking within
329 each time interval (Fig. 8). This divergent behaviour is strongest in BL-NS models
330 (models 3.3, 3.4, 4.3, 4.4) while it is barely discernible in SL-CS models (model 1.1,

331 1.2, 2.1, 2.2). Lobate and distal deposits undergo a more uniform volume of reworking
332 over time.

333 The proportion of the preserved depositional units reaches a reasonably steady state
334 for each delta (Fig. 9). The proportions of different depositional units being preserved,
335 although differing between models, is not a divergent characteristic of delta evolution.
336 Figure 9 shows that across this dataset, the channel deposits contributed 18% to 27%
337 of the total deposited volume, lobate deposits contributed 21% to 34%, overbank
338 deposits contributed 6% to 8% and distal deposits contributed 38% to 49%.

339 The proportion of channel deposits is larger in NS-models compared to their
340 corresponding CS-models. This can be seen from models 4.1, 4.2, 4.3 and 4.4 which
341 have a 2% to 11% larger proportion of channel deposits than models 1.1, 1.2, 1.3 and
342 2.4 respectively (Fig. 9). A larger proportion of channel deposits with more bed load is
343 less pronounced and there are outliers to this trend (e.g., models 4.1 and 2.1 in Fig. 9
344 should strictly have less channel deposits for this trend to hold in all rows).

345 The analyses presented thus far is closely related to the evolution of the channel
346 network and SL- to BL- models (left to right in Figs. 5 - 8) exhibited similar trends
347 behaviour to CS- to NS-models (top to bottom in Figs. 5 t- 8). This relationship
348 reverses for the preservation of lobate deposit, where SL- to BL-models trends (left to
349 right in Figs. 4 - 8) corresponds to NS to CS-models trends respectively (bottom to top
350 in Figs. 4 - 8). The volume of lobate deposits is smaller in SL-models than in BL-
351 models. This can be seen in Fig. 9 where models 1.3, 2.4, 3.4, and 4.4 preserve
352 between 3% and 9% more lobate deposits compared to models 1.1, 2.1, 3.1 and 4.1,
353 respectively. However, larger proportions of lobate deposits are preserved in CS-
354 models compared to NS-models. This can be seen in Fig. 9 where models 1.1, 1.2, 1.3

355 and 2.4 preserve between 1% to 9% more lobate deposits to models 4.1, 4.2, 4.3 and
356 4.4, respectively.

357 Overbank deposits account for only a small proportion (6-8%) of the preserved
358 deposits and is the highest in model 4.1 (Fig. 9). Preserved overbank deposition is
359 higher in systems with non-cohesive sediment supply and systems which favours
360 suspended load transport.

361 Conversely to channel deposits, preserved proportion of distal deposits is larger when
362 suspended load transport is greater. SL-models 1.1, 2.1, 3.1 and 4.1 have a 5% to 9%
363 larger proportion of distal deposits compared to models 1.3, 2.4, 3.4 and 4.4,
364 respectively (Fig. 9). In the distal deposits the correlation with cohesivity is less
365 continuous with outliers to the trend (e.g., model 1.3 should strictly have a larger
366 proportion of distal deposit and model 2.1 less for the trend to hold in all columns).

367 ***3.3 Evolution of delta geometry***

368 The averaged topographic profile of each delta, which represents the overall
369 bathymetry at every output time interval by a single line (Fig. 4), evolves as the delta
370 progrades (Fig. 10).

371 The horizontal brink point displacement is a proxy for delta top progradation. The
372 delta top progrades further into the basin in BL-models than in SL models. This can be
373 seen from the horizontal brink point displacement (Table 2) which is 40% to 80% more
374 in models 2.4, 3.4 and 4.4 compared to models 2.1, 3.1 and 4.1, respectively. No trend
375 on delta top progradation is detected between CS- and NS models.

376 The horizontal delta toe displacement is a proxy for delta front progradation. The delta
377 front progrades further into the basin in CS-models than in NS-models. This can be

378 seen from the horizontal delta toe displacement (Table 2) which is which can be up to
379 three times as much in CS models compared to its respective NS-model (model 1.2
380 compared to model 4.2). The same trend is present between SL-models, where the
381 delta toe can prograde up to twice as far into the basin compared to BL-models (model
382 2.1, SL-model, compared to model 2.4, corresponding BL-model).

383 Proximal vertical displacement was calculated at 2 km distance from the delta apex
384 and serves as a proxy for the level of proximal delta top aggradation. A distance of 2
385 km was chosen as more proximal areas contain too many of the active channel
386 network elements (excluded from the calculation) compared to delta top elements and
387 therefore does not give a representative estimate of the delta top elevation when
388 averaged. The delta top aggrades more in BL-models than in SL-models. Table 2
389 shows that BL models (e.g., models 2.4, 3.4, 4.4) can undergo 40% to 60% more
390 proximal vertical aggradation than their respective SL-models (models 2.1, 3.1, 4.1).
391 The same trend is present for NS-models compared to CS-models, but here the
392 aggradation is only 10% to 30% model in NS-models (e.g., Model 4.1, 4.2 and 4.3)
393 compared to their respective CS models (models 1.1, 1.2, and 1.3).

394 The delta top slope for all models are approximately horizontal, varying between
395 0.04% and 0.05% between models, corresponding to 0.02 degrees to 0.03 degrees.
396 The delta front slopes are steeper than the delta top slopes, starting at approximately
397 0.3% initially, corresponding to 0.2 degrees (Fig. 11). The delta front slopes steepen
398 up to 0.8% (Fig. 11, model 2.4) at the end of the simulation, corresponding to 0.5
399 degrees. The delta front slope steepens faster in BL-models (Fig. 11, dashed lines,
400 models 1.3, 2.4, 3.4 and 4.4) compared to their corresponding SL-models (Fig. 11,
401 solid lines, models 1.1, 2.1, 3.1 and 4.1)

402 In the averaged topographic profiles of some models, degradation stacking (Neal and
403 Abreu, 2009) is observed (Fig 10). This is particularly visible in SL-models (models
404 1.1, 2.1, 3.1 and 4.1) and CS-models (models 1.1, 1.2 and 1.3). This is however an
405 artefact of a longer timescale between channel network avulsions leading to a more
406 rugose shoreline in these models (Model 1.1 compared to Model 1.3, Fig. 5). This is
407 explained in Figure 12, which shows the central lobe in model 1.1 prograding further
408 from the delta apex than the shore-proximal lobes (Fig. 12A interval 50, 12B interval
409 75, 12C interval 100), which produces an apparent degradational averaged
410 topographical profile. Once an avulsion occurs which starts to fill up this shore-
411 proximal bay (Fig. 12D, output time interval 125), the averaged topographic profile
412 begins to even out to a progradational stacking pattern again. Therefore the apparent
413 degradation stacking patterns visible in the averaged topographic profiles are
414 representative of larger timescales for the onset of autogenic events in the models, in
415 particular lobe switching activity. Figure 10 therefore shows that SL- models and CS-
416 models have a larger timescale for the onset of autogenic events than their
417 corresponding BL-models and NS-models.

418 **4 Discussion**

419 We developed and employed a set of general metrics to compare deposits from an
420 ensemble of synthetic deltas. These metrics fall into three categories:

- 421 1. Channel morphology and kinematics,
- 422 2. Sediment reworking and preservation,
- 423 3. Large scale delta geometry.

424 These depositional responses are interdependent, as the evolving system strives to
425 reach optimal hydraulic efficiency.

426 In the prograding systems of the model ensemble, the driving force behind delta
427 evolution is fluvial input, supplied to the delta through the distributary channel network.
428 The evolution of the channel network is therefore key in describing the depositional
429 behaviour of the system. However more distal depositional behaviour, such as the
430 delta front slope and the volume of lobate deposits, shows less correlation to the
431 difference in the channel network morphology and kinematics, and transport and
432 settling behaviour of the sediment becomes more important.

433 We have identified gradual differences in the geometric depositional patterns from bed
434 load (BL) systems to suspended load (SL) systems and we discuss the end-members
435 of these systems separately. BL systems exhibit many, but not all, of the same
436 characteristics as non-cohesive (NS) systems, and the differences and similarities are
437 discussed separately.

438 **4.1 *Suspended load systems***

439 The degree of channel network overlap from one output time interval to the next is a
440 proxy for channel mobility, reflecting both avulsion and lateral migration of channels.

441 Suspended load systems (SL-models) have low channel mobility. The suspended
442 sediment (cohesive plus suspended non-cohesive sediment) in the SL-models can
443 readily bypass the channel network, limiting vertical aggradation within the channels.

444 Channels therefore erode deeper into the underlying delta deposits than in BL-models.

445 Active channels occupy the same location for a longer time, producing localised lobate
446 deposits over and through which the channel progrades into the basin. This leads to a
447 rugose delta brink contour (Fig. 3). After an avulsion occurs in these systems, it leaves

448 a deep abandoned channel feature in the delta top which is initially unfilled but which
449 no longer forms part of the active channel network. Together with the rugose delta
450 brink development, this contributes to a larger variability in delta top geometry in SL-
451 models.

452 The low channel mobility not only affects delta top geometry, but also implies that
453 channels rework a limited area of the delta top. Delta top deposits (channel and
454 overbank) override the older lobate deposits and even older distal deposits. Since SL-
455 models produced deeper channels, channel erosion can reach down to underlying
456 lobate and distal deposits more readily. The extent to which the underlying deposits
457 are reworked also depends on the thickness of the delta top deposits. The low mobility
458 of the channel network produces elongated, prograding channels which transport
459 sediment deeper into the basin. More sediment is transported to the delta front and
460 prodelta rather than being distributed on the delta top. Therefore the delta top does not
461 aggrade, but instead the delta front progrades further into the basin. The reworking of
462 these vertically stacked architectural elements, over a limited horizontal area, could
463 produce a heterogeneous distribution of delta facies, disconnected by the deep
464 channel features.

465 These deep channel features and heterogeneous facies distributions correspond to
466 what has previously been described as a topset-dominated delta (Edmonds et al.,
467 2001). However all the models analysed here fall into the category of foreset-
468 dominated deltas based on their channel depth and foreset-thickness.

469 As suspended sediment transport increases (Fig. 9, right to left), there is a gradual
470 change in sediment dispersal from favouring channel and proximal lobate deposits to
471 increasingly distal deposition. The delta front in SL-models consists of a thin,

472 elongated sediment bed which gradually blends into the prodelta distally. Once
473 deposited, proximal lobate deposits at the delta brink are soon partially reworked by
474 the prograding, low mobility channel from which it was initially deposited. Together
475 with the deeper channels in SL-models which reach down to rework older lobate
476 deposits, the reworking of lobate deposit at the channel mouth causes a smaller
477 proportion of the lobate deposits to be preserved compared to BL-models. The
478 reworked lobate deposits are then redeposited further into the basin or as overbank
479 deposits. This causes the delta toe (and by proxy the delta front) to prograde further
480 into the basin in SL-models. Less delta top aggradation and progradation and more
481 delta front progradation in SL-models leads to elongated clinoforms which steepen at a
482 slower rate than in the corresponding BL-models.

483 In addition, low channel mobility lead to a larger temporospatial scale of autogenic
484 lobe switching events, which can be seen from the apparent degradational clinoforms
485 in the averaged topographical profiles (e.g., Model 1.1 or 2.1, Fig. 10) as explained in
486 Fig. 12.

487 **4.2 Bed load systems**

488 BL-models exhibit highly mobile channel networks with frequent avulsions. The bed
489 load transport constrains sediment to the channel network during both transport and
490 deposition. This causes vertical aggradation, increasing the rate of avulsion.

491 Overloading of bed sediment has previously also been linked to vertical channel
492 aggradation followed by avulsion (e.g., Kleinhans et al., 2012).

493 This means more bed load transport leads to shallower channels features, which
494 contribute to less geometric variability in delta top geometry than the deep channels of
495 the SL-models. In addition, the highly mobile channel network distributes sediment

496 smoothly across the entire delta front and delta top creating a smooth delta brink
497 contour (Fig. 5, models 1.3, 2.4, 3.4 and 4.4 compared to models 1.1, 2.1, 3.1 and 4.1,
498 respectively). Repeated reworking by the channel network in the BL-models further
499 smooths delta top geometry.

500 Together with the smooth, reworked delta top, the vertical aggradation in the channel
501 network causes the entire delta top to aggrade over time. This is most pronounced at
502 proximal locations, which have undergone aggradation and reworking for a longer
503 period than the distal locations. The rise in proximal floodplain elevation in the
504 simulations leads to a rise in water level. This creates additional accommodation in
505 inter-distributary/bay areas, which future channel avulsions may occupy. It is not
506 possible to isolate whether the aggradation drives the channel dynamics or whether
507 the channel dynamics drive the aggradation. Most likely the channel dynamics and
508 delta top aggradation create a constructive feedback effect in high bed load systems.

509 The channel mobility in systems characterised by bed load transport causes a large
510 area of the delta top to be reworked by the channels. The shallow channels do not
511 frequently erode into the underlying lobate and or distal deposits. Therefore reworking
512 is mainly constrained to the upper layers of channel and overbank deposits which
513 constitute the delta top. This leads to a more uniformly stacked stratigraphy of distal
514 deposits, overridden by lobate deposits, which in turn is overridden by a mixture of
515 channel and overbank deposits which at the delta top. This homogeneous geometry
516 and distribution of depositional units is consistent with that described for foreset-
517 dominated deltas (Edmonds et al., 2011).

518 Bed load not deposited in active channel network is transported towards the channel
519 mouth where it is deposited as lobate deposits. When the downstream distance along

520 the channel becomes too large for sediment to be transported to the channel mouth,
521 channels aggrade vertically, eventually leading to avulsion (Kleinhans et al., 2012).
522 This increases the proportion of sediment deposited close to the channel network
523 (channel and proximal lobate deposit) at the expense of overbank and distal deposits.
524 The shallower, aggradational channels are also less likely to rework lobate deposits at
525 the channel mouth or reach down to it as the channels traverse the delta top.
526 Therefore BL-models preserve a larger quantity of especially proximal deposits.
527 This preferential proximal deposition means that more bed load transport in a deltaic
528 system causes more delta top aggradation and progradation and less delta front
529 progradation into the basin. This also increases the rate at which the delta front slope
530 steepens as the delta progrades into the basin. The clinofolds in BL-deltas are
531 smooth (Fig. 10) compared to those in SL-models, indicating a shorter temporospatial
532 scale of autogenic lobe switching events than in SL-models.

533 ***4.3 The role of sediment transport compared to cohesive sediment supply on*** 534 ***deltaic deposition***

535 Based on the analyses presented, kinematics, channel morphology and channel
536 deposits undergo a similar shift in behaviour if the proportion of suspended load is
537 greater (SL-models) or if the proportion cohesive sediment is greater (CS-models). In
538 both these of these cases channels will be deeper, channel kinematics will be less,
539 leading to less delta top reworking, a more heterogeneous geometric distribution of
540 depositional units, and a more rugose shoreline. Low channel mobility such as that
541 seen in SL-models, has also previously been associated with cohesive sediment
542 (Edmonds and Slingerland, 2009; Hoyal and Sheets, 2009; Edmonds et al., 2011;
543 Geleynse et al., 2011).

544 In the case of suspended load systems, however, the preserved proportion of channel
545 deposits is only weakly correlated with decrease in channel kinematics and the
546 proportion of lobate deposit is also less with lower channel kinematics. In the case of
547 cohesive systems, however, this correlation between channel kinematics and channel
548 deposits is strong, but an increase in lobate deposits is observed rather than the
549 decrease seen in suspended load systems.

550 We also observe no trend in delta front progradation between models where only the
551 cohesivity is varied, although there is a very strong change in delta front progradation
552 with increasing cohesivity (Fig. 10, compare models in each column). On the other
553 hand, there is a definite increase in delta top progradation with increasing bed load
554 transport, but a smaller correlation of sediment transport with delta toe progradation
555 (Fig. 10, compare the models in each row).

556 In order to understand the above similarities and differences, we need to understand
557 the difference between varying the proportion of cohesive sediment supply compared
558 to varying the proportion of suspended load transport in the simulations. The average
559 sediment supply D_{50} is lower in cohesive compared to non-cohesive simulations (Table
560 1), while the balance between suspended load and bed load only changes the
561 transport mechanism and not the D_{50} of the sediment supply. Smaller grain sizes
562 mean lower settling velocities and therefore more sediment bypasses the delta top,
563 depositing as lobate and distal deposits in the delta front and prodelta positions
564 instead. Similar responses to grain size have been recorded in the literature (Caldwell
565 and Edmonds, 2014).

566 Our findings indicate that while both suspended load and cohesive sediment can
567 change the distributary network morphodynamics in the same way, they influence

568 deposition more distal from the network in distinctly different ways. Sediment supply
569 composition is shown to change the progradation of the delta front while not exhibiting
570 a clear trend in delta top progradation or delta front slope. Sediment transport
571 mechanism was shown to strongly influence the rate at which the delta front steepens
572 and the delta top progrades, while more weakly influencing the progradation of the
573 delta front.

574 **4.4 From synthetic analogues to natural systems**

575 The model results are presented as synthetic analogues to analyse the effects of
576 sediment transport on the general depositional behaviour in natural systems. This
577 requires consideration of the differences between the synthetic analogues and natural
578 systems.

579 We investigate variations in the mechanism of sediment transport (suspended vs. bed
580 load) independently from variation in sediment cohesivity. However, in natural deltaic
581 systems these two aspects are related. Bed load transport in deltaic systems is still
582 poorly understood and it has been suggested that it should not be calculated as a
583 function of suspended load but as a separate entity (Kazemi et al., 2012).

584 One process which has been linked to the proportion of bed load transport in fluvial
585 systems is flooding (Karimae Tabarestani and Zarrati, 2015). Our simulations impose
586 constant discharge, which limits the amount of channel over-spilling, and may
587 underestimate overbank deposition. Due to the link between floods and higher
588 proportions of bed load transport, an underestimation of overbank deposits is likely
589 more relevant for systems with high bed load transport (BL-models). At the same time,
590 we do not model low stage discharge, which would be dominated mainly by

591 suspended load. During these low discharges, overbank deposits are unlikely to be
592 generated and the models could therefore also overestimate overbank deposition.

593 In natural systems the relationship between suspended load and bed load is not
594 constant (Laronne and Reid, 1993; Chatanantavet et al., 2012; Karimae Tabarestani
595 and Zarrati, 2015). During peak flow events, bed load transport may constitute a much
596 higher proportion of the total load (Turowski et al., 2010). Lamb et al. (2012) suggest
597 that flooding can increase erosion in the backwater region. We assume a constant
598 flooding stage, which lacks the base flow discharge. Future work could investigate the
599 effect that varying flow between flooding and base discharge has on the balance
600 between aggradation and erosion of the floodplain and subaqueous delta top.

601 We identified different patterns of aggradation, progradation and retrogradation in the
602 averaged topographic profiles (Fig. 10) which match with some of the patterns
603 described in Neal and Abreu (2009). However, our simulations represent at most
604 deposition on an intraparasequence scale. By the end of the simulations the delta front
605 slope reaches between 0.3° and 0.5° , which is considered shallow for a delta front
606 slope (Korus and Fielding, 2015). However the delta front slopes are still increasing,
607 and therefore for longer simulations or a steeper initial basin slope it is expected that a
608 steeper delta front slope would be reached.

609 All heterogeneities in the geometry and stratigraphy of the simulation are driven by
610 autogenic self-organisation of the depositional system. The delta front slopes of the
611 different models steepen at different rates, and it is therefore postulated that the
612 difference in delta front slope between the different models will diverge further for
613 longer simulations, at least up to the autobreak point (Muto et al., 2007). The constant
614 sediment supply and zero change in accommodation corresponds to sealevel stillstand

615 as described by Muto et al. (2007). However our simulations do not prograde long
616 enough to reach an autobreak. The lower rate of steepening in the suspended load
617 systems also means that sediment is spread over a larger area and therefore it may
618 reach an autobreak point earlier than a corresponding system with large proportions of
619 bed load transport.

620 The set of metrics presented here allow objective comparison of the evolution of
621 deltaic deposits in four dimensions. When comparing model results, we are able to
622 vary a single variable and study its influence in great detail between consistent
623 experiments. Databases comparing modern deltaic systems investigates deposition in
624 geomorphological sub-environments and considers predictive controls on their
625 morphodynamics (Syvitski and Saito, 2007; Korus and Fielding, 2015). These natural
626 systems respond to the interaction of a wide range of boundary conditions (e.g.,
627 climate, accommodation space, sediment transport, discharge, marine processes,
628 river power, wave energy, tidal energy). In addition deposition responds to the number,
629 magnitude and sequence of events occurring during deposition (e.g., floods,
630 tectonism, sealevel changes) (Syvitski and Saito, 2007). Due to this large variety of
631 influencing factors, a comparison of natural systems does not allow the definitive
632 association of depositional patterns to differences in a single boundary condition. The
633 strength of a process-based modelling approach, as presented here, is that it allows
634 the analysis of depositional responses to changes in a single variable.

635 **5 Conclusions**

636 The mechanism of sediment transport was shown to have at least as big an impact on
637 delta kinematics, morphology and stratigraphy as sediment cohesivity. When sediment
638 cohesivity remains constant, morphology previously associated with sediment

639 cohesivity could also be produced by increasing the proportion of suspended load
640 sediment transport. Differences in channel kinematics can be due to the mechanism of
641 sediment transport or the supply composition. We found channel kinematics to be a
642 key factor in predicting the evolution of proximal depositional patterns in deltas, but
643 that distal depositional trends respond differently to changes in sediment supply and
644 sediment transport mechanisms.

645 The similarities between the depositional responses of bed load systems and non-
646 cohesive sediment supply highlight how a deltaic sediment body can originate from a
647 non-unique sequence of depositional controls and events. During the dynamic
648 evolution of a delta's stratigraphy and morphology numerous processes and controls
649 interact. While calculated values for bed load transport for modern systems have been
650 reported in databases of modern deltaic systems (Syvitski and Saito, 2007; Korus and
651 Fielding, 2015), our models highlight the influence of these sediment transport
652 mechanisms on long term delta evolution. In addition to sediment budget and
653 sediment supply composition, the effect of the mechanism of sediment transport, and
654 its geometric implication on the preserved stratigraphy, should be considered when
655 creating geological models of deltaic deposits.

656 Previous authors stated that models prograding during a sealevel stillstand (as in our
657 simulations) do not have a characteristic temporospatial scale for autogenic events
658 due an ever-decreasing rate of progradation (Muto et al., 2007). However in our
659 simulations, bed load systems and non-cohesive systems undergo more frequent and
660 smaller autogenic reorganisations than suspended load systems and cohesive
661 systems. If it is true that the stratigraphic products of large scale autogenic processes
662 can easily be misinterpreted as those of allogenic processes (Muto et al., 2007), then

663 our work suggests that this risk is higher in systems which high suspended load or
664 higher levels of cohesive sediment supply.

665 We conclude that a better insight into the ratio of bed- to suspended load is crucial to
666 predicting morphologic and stratigraphic aspects of a delta.

667 **Acknowledgements**

668 This work received financial support from Deltares and Shell. The simulations were
669 carried out on the Dutch national e-infrastructure with the support of SURF Foundation
670 (NWO project MP-293-14). We would like to thank Liang Li for many useful
671 discussions during the development of this work, Bert Jagers for his help answering
672 questions relating to Delft3D and Matthew Wolinsky for help during the development of
673 the analysis. We would also like to thank the two anonymous reviewers for their
674 feedback, which helped to improve the text.

675 **References**

676 Ashworth, P.J., Lewin, J., 2012. How do big rivers come to be different? *Earth-Science*
677 *Reviews* 114, 84–107.

678 Caldwell, R.L., Edmonds, D.A., 2014. The effects of sediment properties on deltaic
679 processes and morphologies: A numerical modeling study. *Journal of Geophysical*
680 *Research: Earth Surface*, 119, 961–982.

681 Edmonds, D.A., Slingerland, R.L., 2009. Significant effect of sediment cohesion on
682 delta morphology. *Nature Geoscience* 3, 105–109.

683 Edmonds, D.A., Shaw J.B., Mohrig, D., 2011. Topset-dominated deltas: A new models
684 for river delta stratigraphy. *Geology* 29, 1175-1178.

685 Engelund, F., Hansen, E., 1967. A monograph on Sediment Transport in Alluvial
686 Streams. Teknisk Forlag, Skelbreggade 4, Copenhagen V, Denmark, 59pp.

687 Galappatti, R., 1983. A depth integrated model for suspended transport. Delft
688 University of Technology, Delft, The Netherlands, 111pp.

689 Galloway, W.D., 1975. Process Framework for describing the morphologic and
690 stratigraphic evolution of deltaic depositional systems. In: Deltas: Models for
691 Exploration. Houston Geological Society, Houston, USA, pp. 86–98.

692 Geleynse, N., Storms, J.E.A., Stive, M.J.F., Jagers, H.R.A., Walstra, D.J.R., 2010.
693 Modeling of a mixed-load fluvio-deltaic system. *Geophysical Research Letters* 37,
694 doi:10.1029/2009GL042000

695 Geleynse, N., Storms, J.E.A., Walstra, D.J.R., Jagers, H.R.A., Wang, Z.B., Stive,
696 M.J.F., 2011. Controls on river delta formation; insights from numerical modelling.
697 *Earth and Planetary Science Letters* 302, 217–226.

698 Geleynse, N., Voller, V.R., Paola, C., Ganti, V., 2012. Characterization of river delta
699 shorelines. *Geophysical Research Letters* 39, doi:10.1029/2012GL052845

700 Gibling, M.R., 2006. Width and Thickness of Fluvial Channel Bodies and Valley Fills in
701 the Geological Record: A Literature Compilation and Classification. *Journal of*
702 *Sediment Research* 76, 731–770.

703 Guo, L., van der Wegen, M., Roelvink, D.J.A.A., Wang, Z.B., He, Q., 2015. Long-term,
704 process-based morphodynamic modeling of a fluvio-deltaic system, part I: The role of
705 river discharge. *Continental Shelf Research* 109, 95–111.

706 Hajek, E.A., Wolinsky, M.A., 2012. Simplified process modeling of river avulsion and
707 alluvial architecture: Connecting models and field data. *Sedimentary Geology* 257-260,
708 1–30.

709 Howell, J. A., Skorstad, A., MacDonald, A., Fordham, A., Flint, S., Fjellvoll, B.,
710 Manzocchi, T., 2008. Sedimentological parameterization of shallow-marine reservoirs.
711 *Petroleum Geoscience* 14, 17-35.

712 Hoyal, D.C.J.D., Sheets, B.A., 2009. Morphodynamic evolution of experimental
713 cohesive deltas. *Journal of Geophysical Research: Earth Surface* 114(F2),
714 doi:10.1029/2007JF000882

715 Jerolmack, D.J., Mohrig, D., 2007. Conditions for branching in depositional rivers.
716 *Geology* 35, 463–466.

717 Karimae Tabarestani, M.K., Zarrati, A.R., 2015. Sediment transport during flood
718 event: a review. *Journal of Environmental Science and Technology* 12, 775–788.

719 Korus, J.T., Fielding, C.R., 2015. Asymmetry in Holocene river deltas: Patterns,
720 controls, and stratigraphic effects. *Earth-Science Reviews* 150, 219-242.

721 Kleinhans, M.G., 2010. Sorting out river channel patterns. *Progress in Physical*
722 *Geography* 34, 287–326.

723 Kleinhans, M.G., de Haas, T., Lavooi, E., Makaske, B., 2012. Evaluating competing
724 hypotheses for the origin and dynamics of river anastomosis. *Earth Surface Processes*
725 *and Landforms* 37, 1337–1351.

726 Kleinhans, M.G., Grasmeijer, B.T., 2006. Bed load transport on the shoreface by
727 currents and waves. *Coastal Engineering* 53, 983–996.

728 Laronne, J.B., Reid, I., 1993. Very high rates of bedload sediment transport by
729 ephemeral desert rivers. *Nature* 366, 148–150.

730 Lesser, G.R., Roelvink, D.J.A., van Kester, J.A.T.M., Stelling, G.S., 2004.
731 Development and validation of a three-dimensional morphological model. *Coastal*
732 *Engineering* 51, 883–915.

733 Maddock, T., Borland, W.M., 1950. *Sedimentation Studies for the Planning of*
734 *Reservoirs by the Bureau of Reclamation. Technical Report, United States*
735 *Department of the Interior, Bureau of Reclamation, Branch of Project Planning.*

736 Milliman, J.D., Farnsworth, K.L., 2011. *River Discharge to the Coastal Ocean: A*
737 *Global Synthesis. Cambridge University Press, Cambridge, 382pp.*

738 Muto, T., Steel, R.J., Swenson, J.B., 2007. Autostratigraphy: A framework norm for
739 genetic stratigraphy. *Journal of Sedimentary Research* 77, 2-12.

740 Neal, J., Abreu, V., 2009. Sequence stratigraphy hierarchy and the accommodation
741 succession method. *Geology* 37, 779-782.

742 Orton, G.J., Reading, H.G., 1993. Variability of deltaic processes in terms of sediment
743 supply , with particular emphasis on grain size. *Sedimentology* 40 475–512.

744 Paola, C., Straub, K., Mohrig, D., Reinhardt, L., 2009. The “unreasonable
745 effectiveness” of stratigraphic and geomorphic experiments. *Earth-Science Reviews*
746 97, 1–43.

747 Peakall, J., Ashworth, P.J., Best, J.L., 2007. Meander-Bend Evolution, Alluvial
748 Architecture, and the Role of Cohesion in Sinuous River Channels: A Flume Study.
749 *Journal of Sediment Research* 77, 197–212.

750 Ranasinghe, R., Swinkels, C., Luijendijk, A., Roelvink, D.J.A., Bosboom, J., Stive,
751 M.J.F., Walstra, D.J.R., 2011. Morphodynamic upscaling with the MORFAC approach:
752 Dependencies and sensitivities. *Coastal Engineering* 58, 806–811.

753 Syvitski, J. P. M., Saito, Y., 2007. Morphodynamics of deltas under the influence of
754 humans. *Global and Planetary Change* 57, 261-282.

755 Turowski, J.M., Rickenmann, D., Dadson, S.J., 2010. The partitioning of the total
756 sediment load of a river into suspended load and bedload: A review of empirical data.
757 *Sedimentology* 57, 1126–1146.

758 van Rijn, L.C., 2007. Unified View of Sediment Transport by Currents and Waves. I:
759 Initiation of Motion, Bed Roughness, and Bed-Load Transport. *Journal of Hydraulic*
760 *Engineering* 133, 649-667

761 van Rijn, L.C., 1993. Principles of sediment transport in rivers, estuaries and coastal
762 seas. Aqua publications, Amsterdam, The Netherlands.

763 **Figure captions**

764 Fig. 1. Bathymetry and boundary conditions for all models in the simulation ensemble
765 with sample simulation output for model 2.3 (top right). The input boundary conditions
766 include discharge and sediment input at the fluvial boundary and a semi-diurnal tide at
767 the distal basin boundary.

768 Fig. 2. Variation in boundary conditions for the models used in this study. Sediment
769 transported as bed load (orange) increases from left to right at the expense of
770 suspended load (blue). The proportion of non-cohesive sediment supply (yellow)
771 increased downwards at the expense of cohesive sediment (brown). Total load

772 concentration is constant at 0.2 kg/m^3 across all models. Model 1.4 does not exist as it
773 is not possible to define 35% bed load from only 30% non-cohesive sediment.

774 Fig. 3. Distribution of preserved depositional units at the end of simulation for Model
775 2.3

776 Fig. 4. Illustration of the construction of the averaged topographic profiles. (A) The
777 original and example output bathymetry of a single output time interval in one model.
778 (B) Elevation of the non-channel bathymetry points averaged radially around the delta
779 apex, plotted as a function of distance from apex to create a single averaged
780 topographic profile (C). (D) For each profile a delta toe and delta brink point is
781 identified which defined the geometric regions delta top, delta front and prodelta. (E)
782 The process is repeated at each time interval and plotted for every 25th time interval,
783 with blue being the oldest profile and orange the youngest.

784 Fig. 5. Bathymetry of model ensemble at the end of the simulation. Elevation values
785 were normalised for localised differences in water level.

786 Fig. 6. Channel network area with percentage of the active channel network area
787 overlapping with that of the previous time interval indicated in yellow. The mean
788 overlap (%) is calculated and illustrated as an orange line. Mean channel depth (m)
789 with respect to the adjacent delta top/flood plain is displayed in the bottom right corner
790 of each graph.

791 Fig. 7. Total volume of sediment deposited over time for all 15 models (blue plus
792 orange area), as it evolves over time. The blue area represents the volume which is
793 eroded (reworked) in each time interval and the orange area the net volume of
794 sediment deposited/preserved per time interval as the delta progrades.

795 Fig. 8. Composition of the reworked sediment by depositional units.

796 Fig. 9. Evolution of total preserved deposit throughout the simulation, by depositional
797 units. The average proportions of channel and delta front deposits at the end of the
798 simulation are also shown.

799 Fig. 10. Evolution of averaged topographic profile of each model over time. Fourteen
800 of the 366 topographic profiles spanning the evolution of each simulated delta are
801 displayed. Blue shows the oldest profile and orange the youngest.

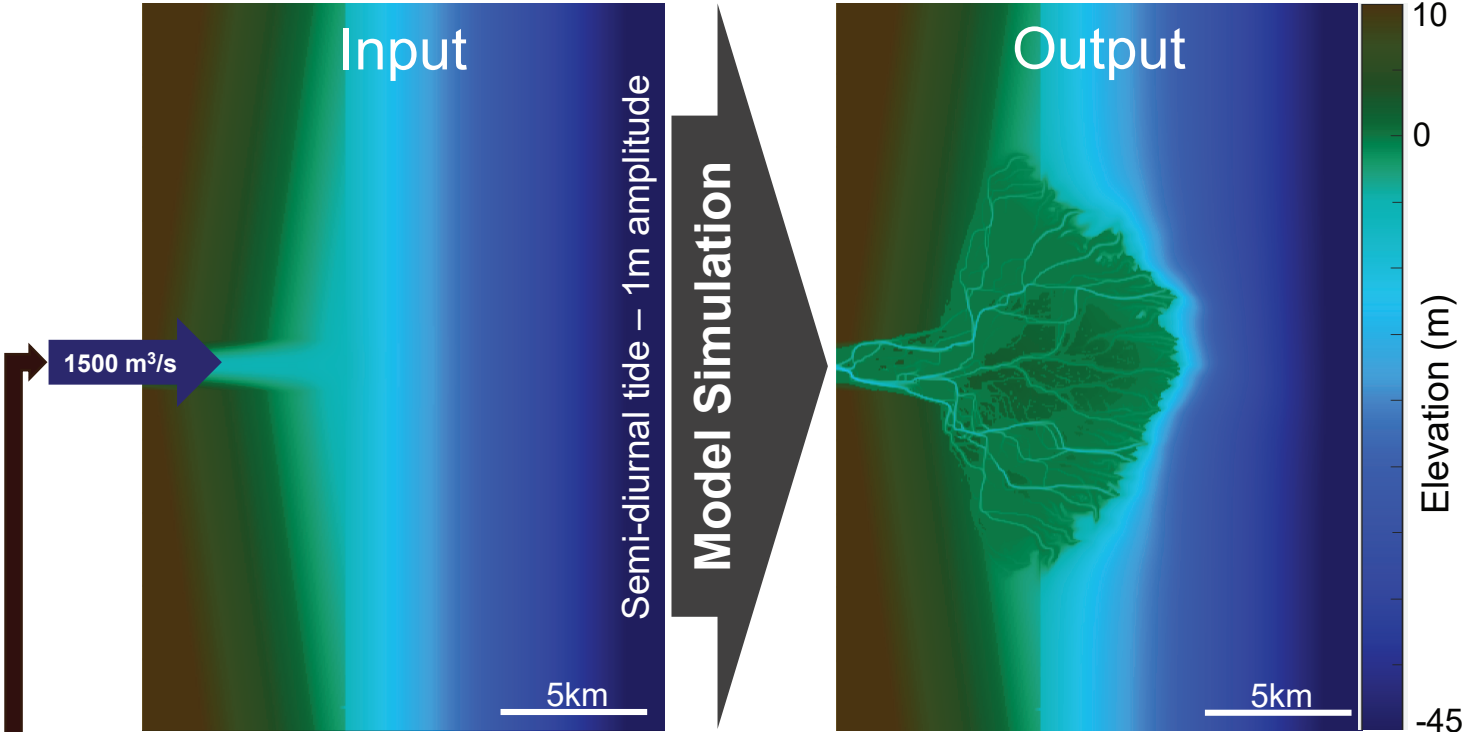
802 Fig. 11. The change in delta front slope over time for all simulations

803 Fig. 12. Averaged topography of time steps 50, 75 and 100 show apparent
804 retrogradation driven by the evolution of the central lobes of the delta (respectively A,
805 B, C) while the lateral lobes have not yet evolved. By time step 125 at least one lateral
806 lobe has started evolving after a major avulsion event, causing the averaged
807 topographical profile to level out and exhibit a progradation pattern.

808 **Table titles**

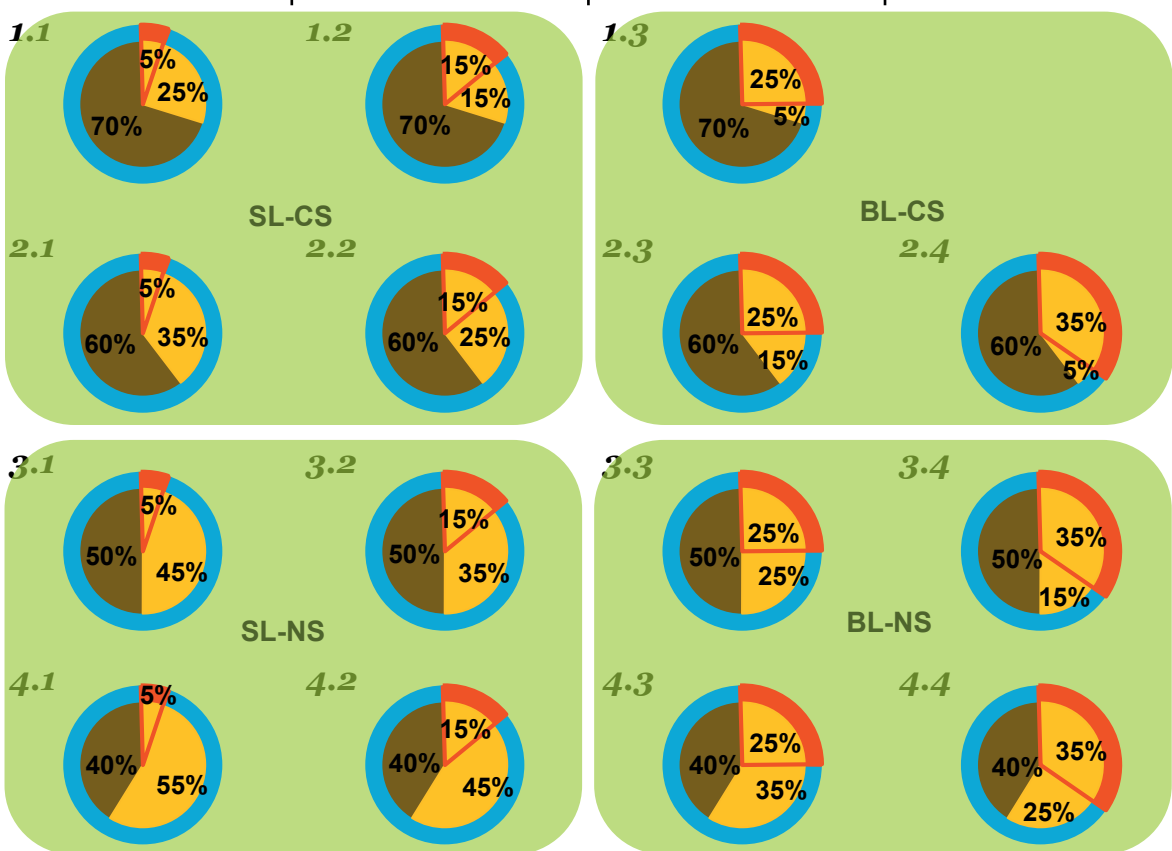
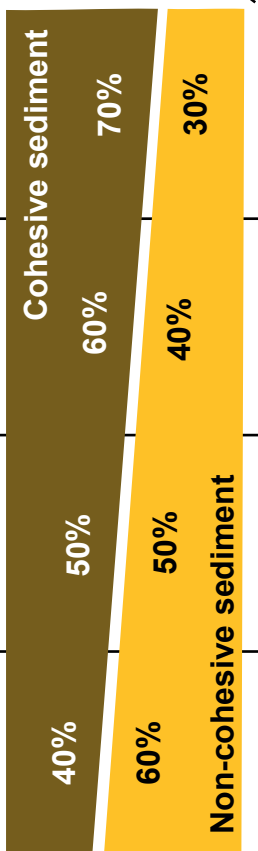
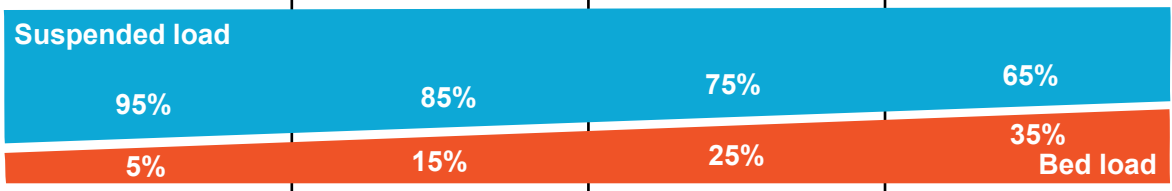
809 Table 1. Input sediment concentrations for all models as well as the resulting D_{50}
810 values.

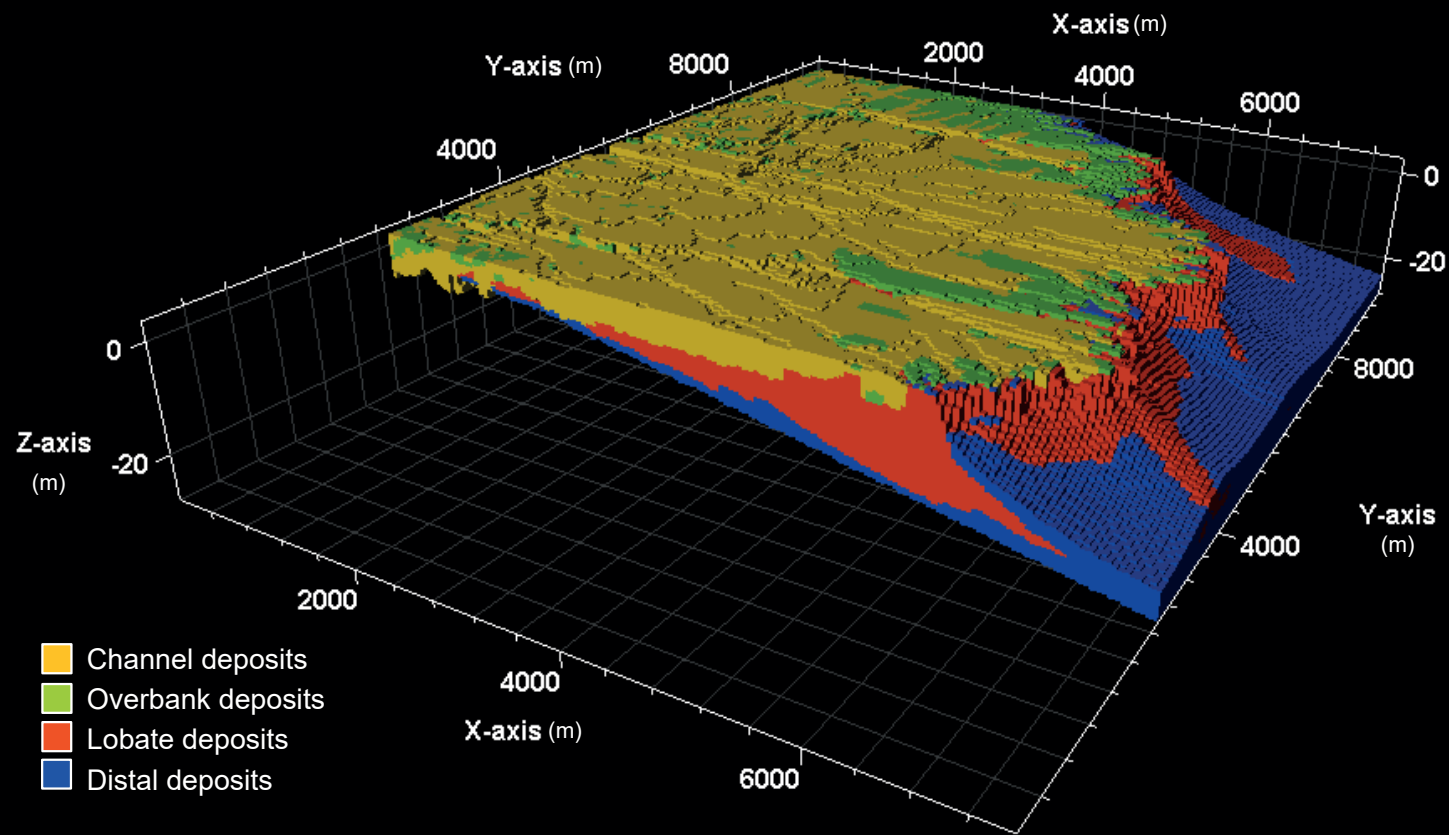
811 Table 2. Values for cumulative vertical aggradation at 2 km from the delta apex and
812 cumulative horizontal displacement for the delta brink and delta toe.

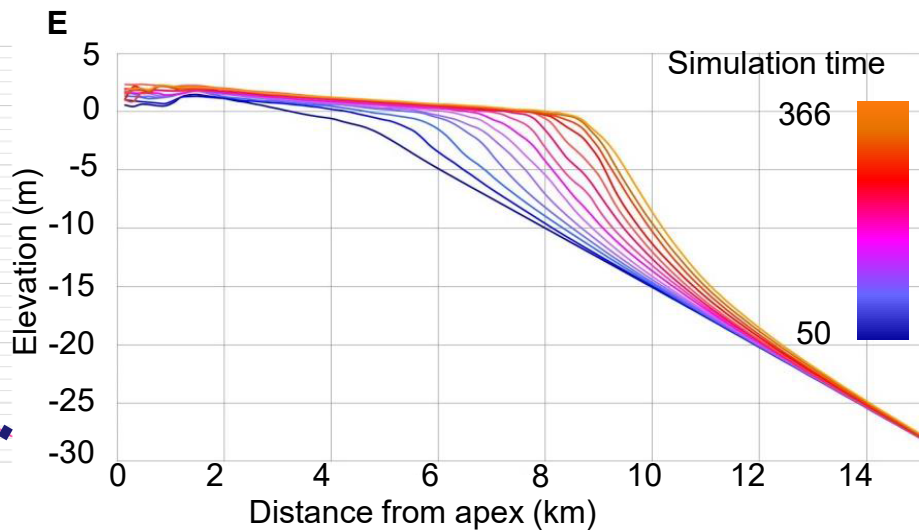
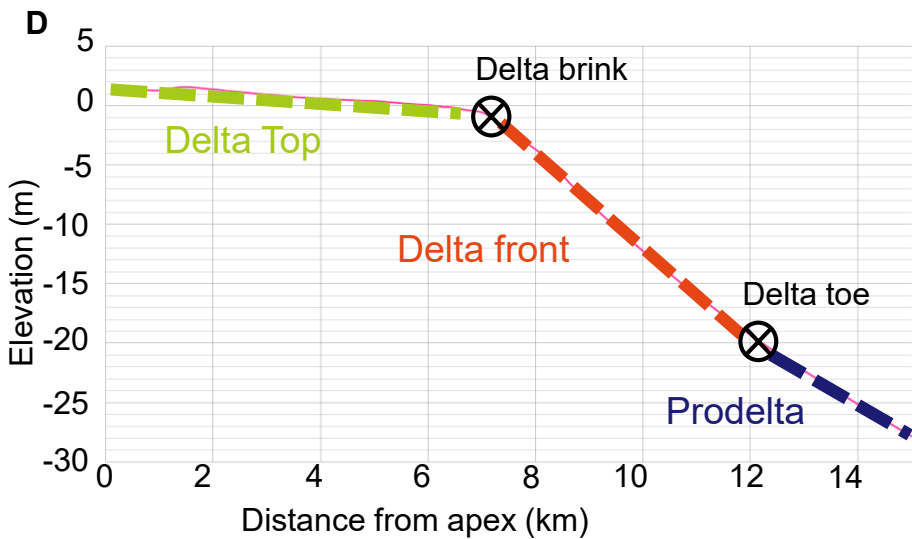
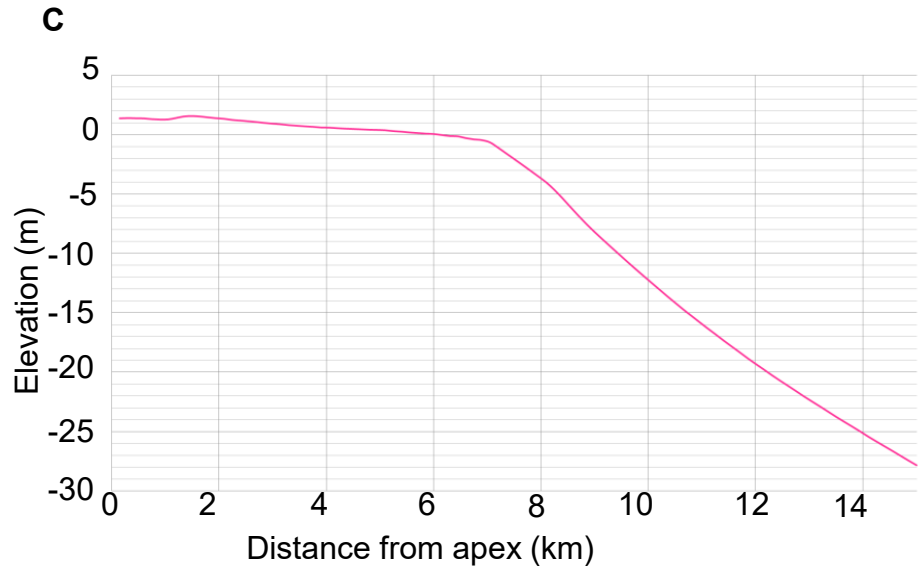
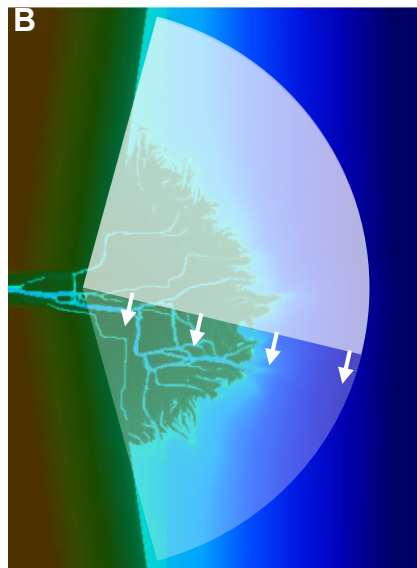
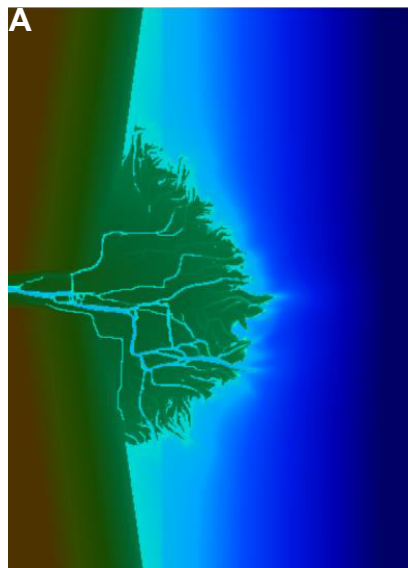


Sediment Class	Median grain size (μm)	Settling Velocity (mm/s)	Critical bed shear stress for sedimentation (N/m^2)	Critical bed shear stress for erosion (N/m^2)	Reference density for hindered settling (kg/m^3)	Specific density (kg/m^3)	Dry bed density (kg/m^3)
Non-Cohesive1	200	-	-	-	1600	2650	1600
Non-Cohesive2	100	-	-	-	1600	2650	1600
Cohesive1	-	0.86	1000	0.3	1600	2650	500
Cohesive2	-	0.25	1000	0.5	1600	2650	500

Sediment
transport
Supply
Composition







Sediment
transport
Supply
Composition

Suspended load (SL)

95%

85%

75%

65%

5%

15%

25%

35%
Bed load (BL)

Cohesive sediment (CS)

70%

30%

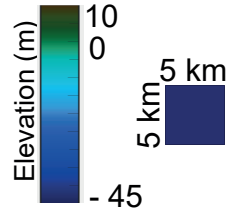
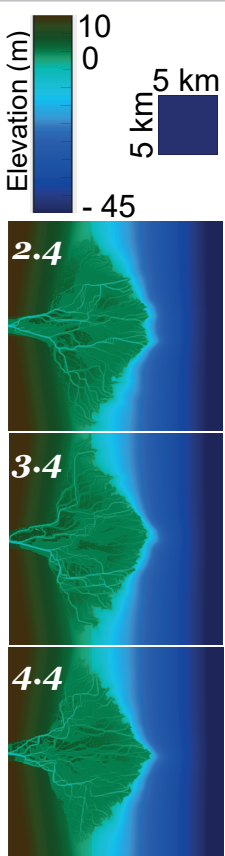
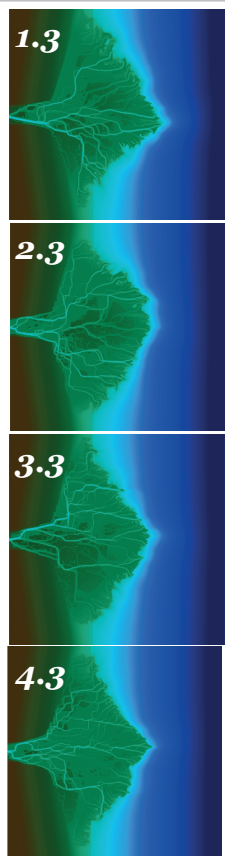
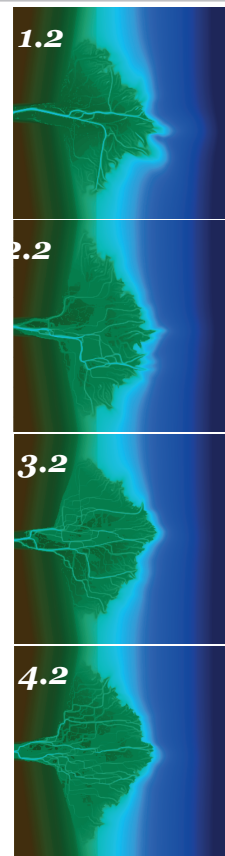
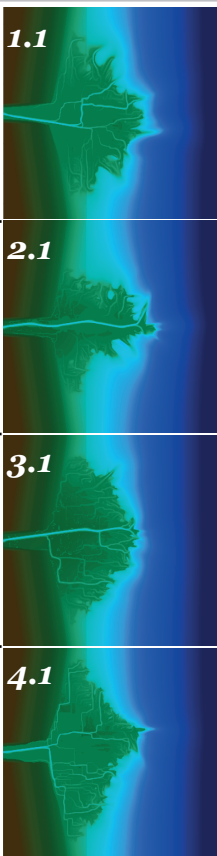
50%

40%

Non-cohesive sediment (NS)

40%

60%

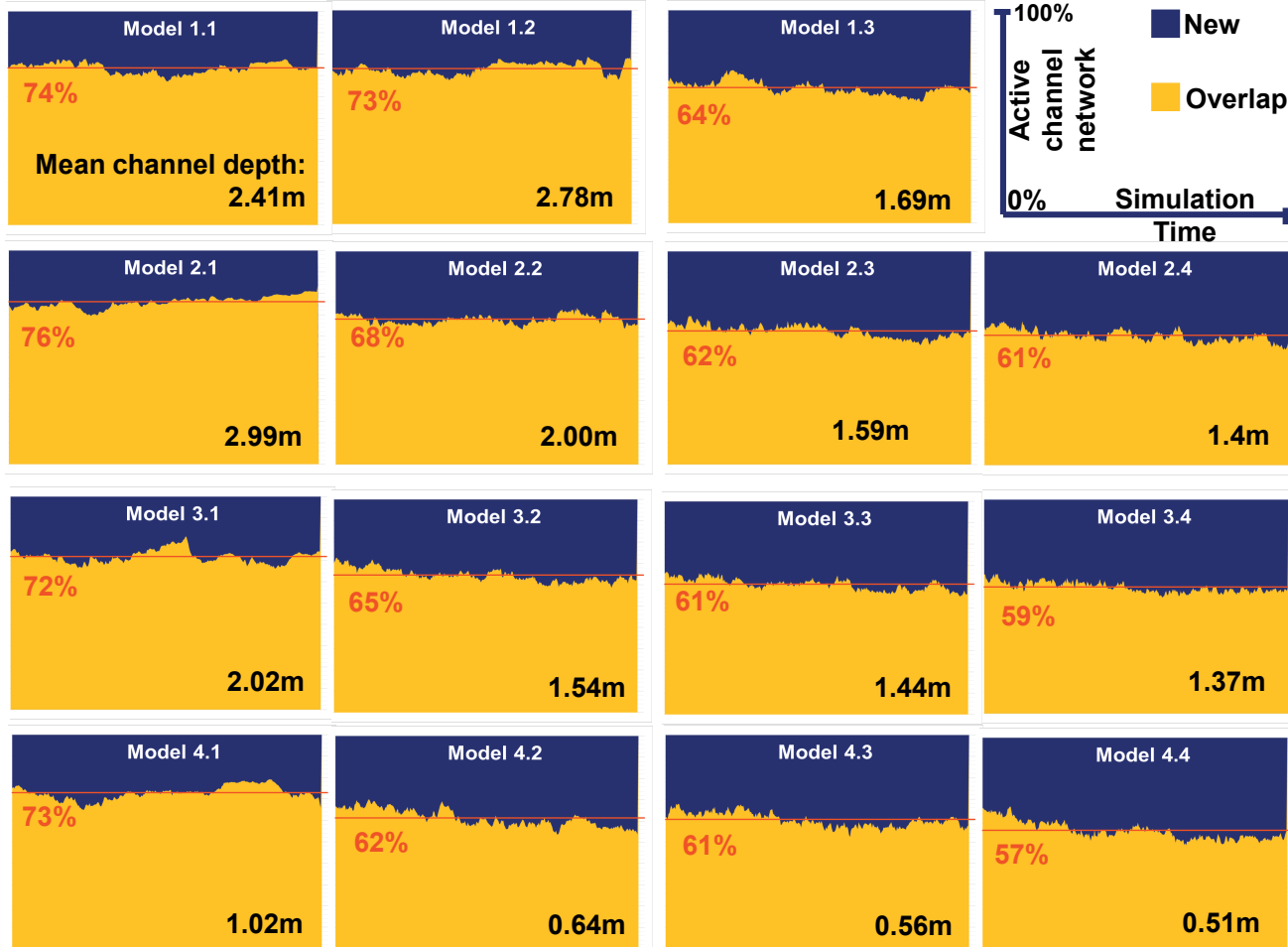


Suspended load (SL)

Bed load (BL)

Cohesive sediment (CS)

Non-cohesive sediment (NS)

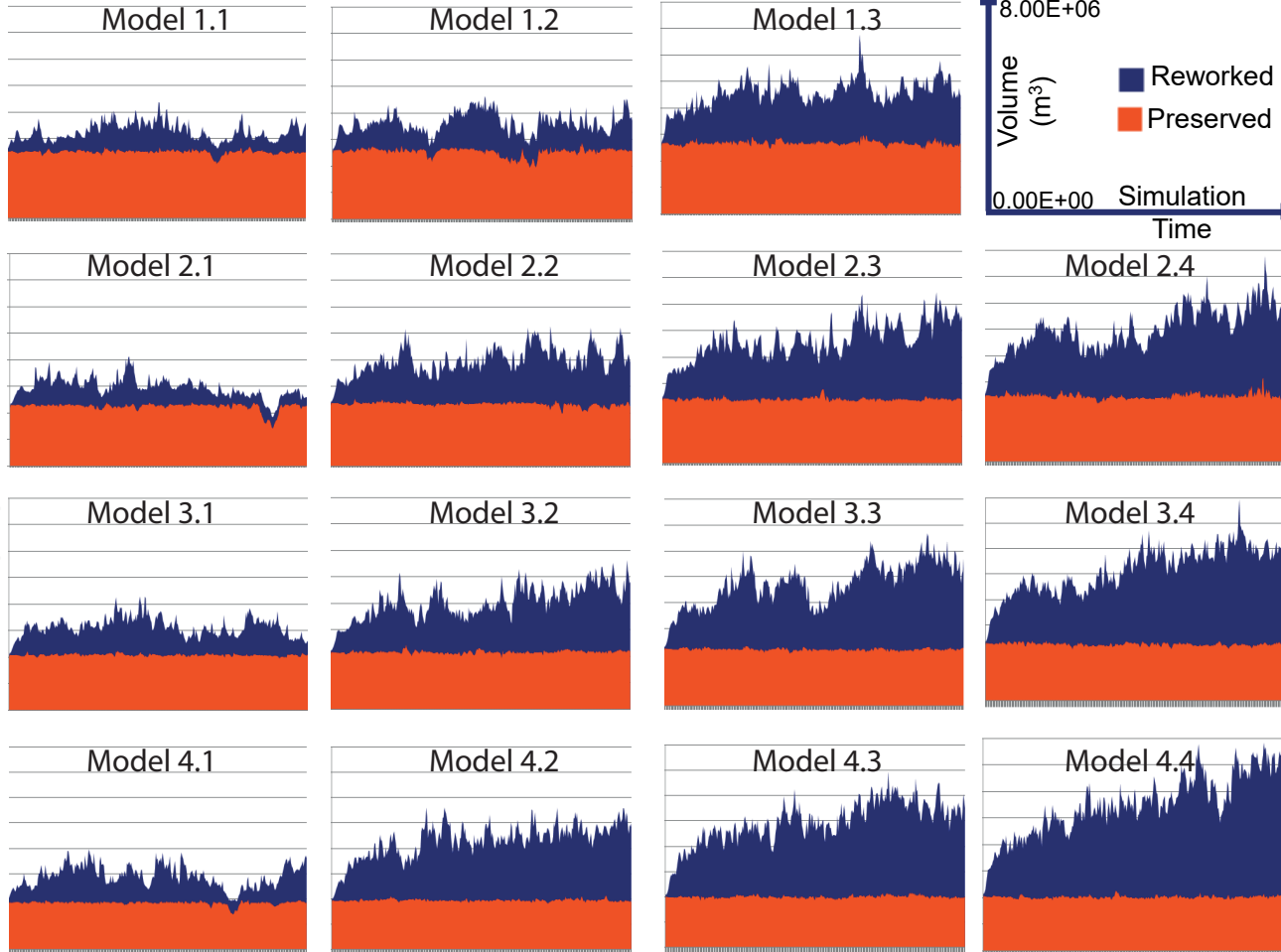


Suspended load (SL)

Bed load (BL)

Cohesive sediment (CS)

Non-cohesive sediment (NS)

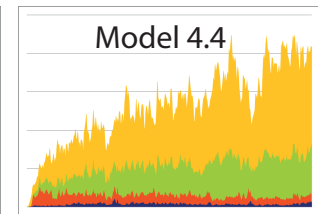
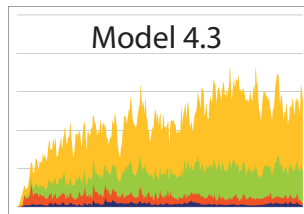
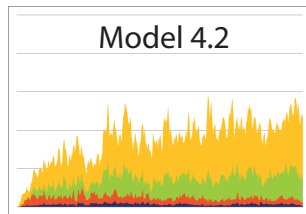
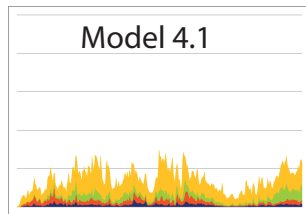
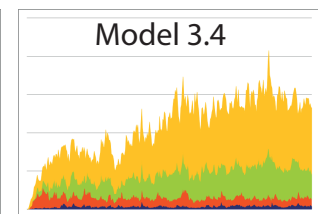
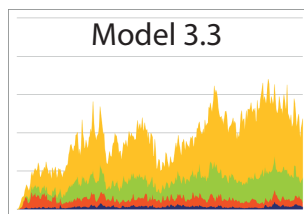
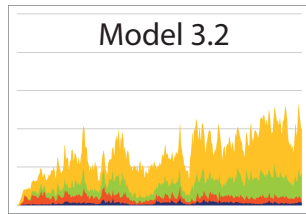
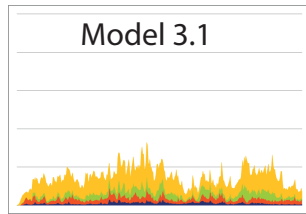
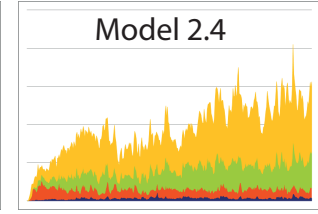
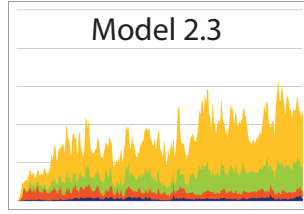
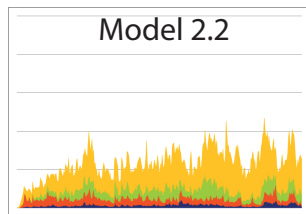
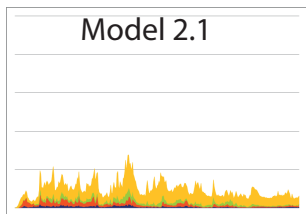
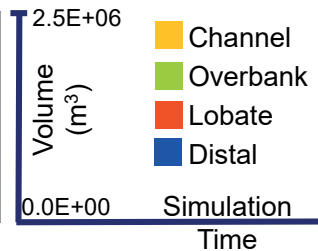
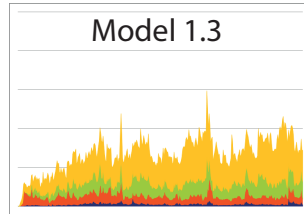
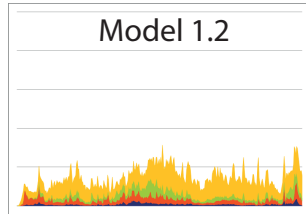
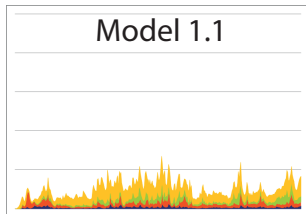


Suspended load (SL)

Bed load (BL)

Cohesive sediment (CS)

Non-cohesive sediment (NS)

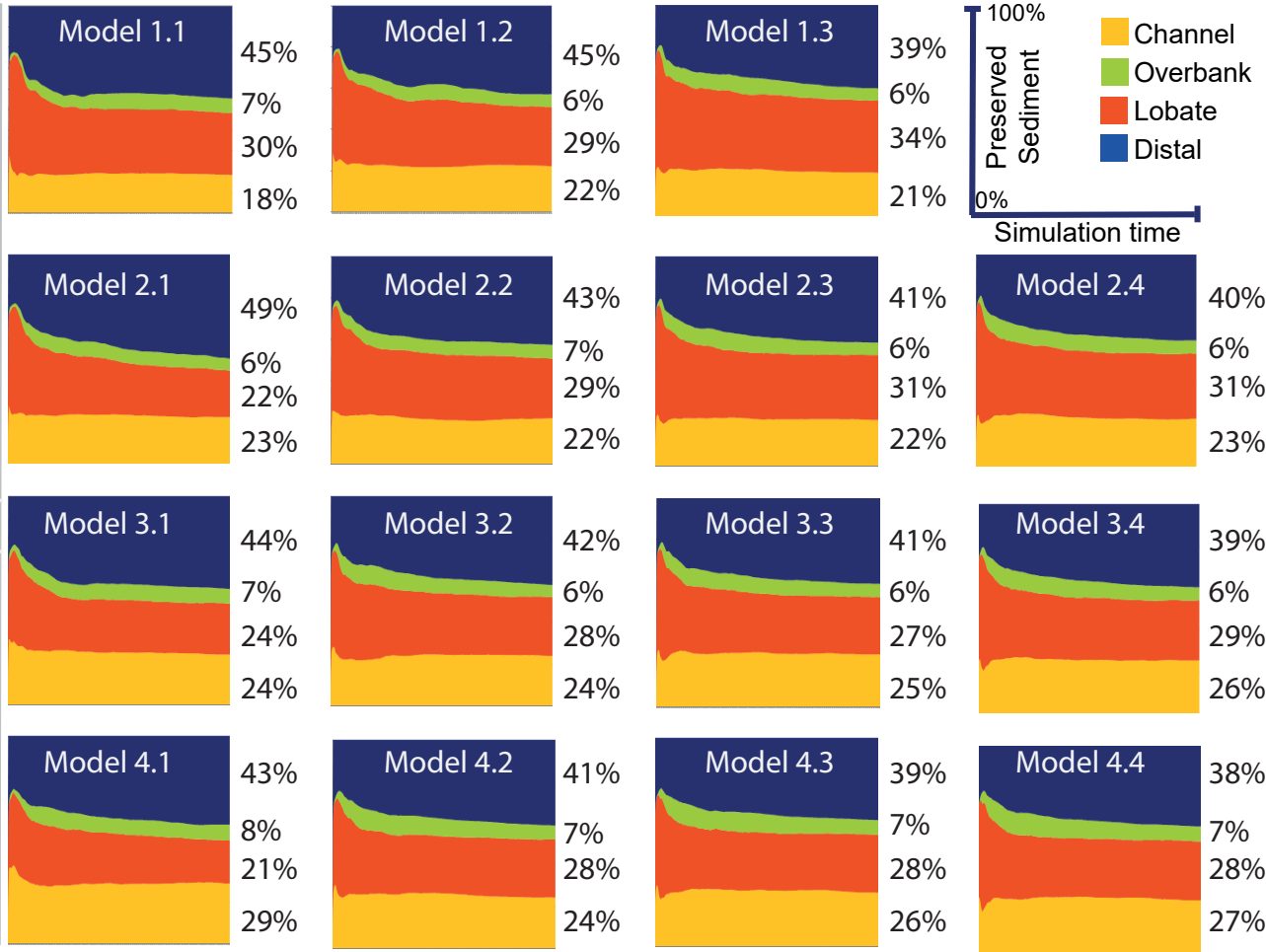


Suspended load (SL)

Bed load (BL)

Cohesive sediment (CS)

Non-cohesive sediment (NS)



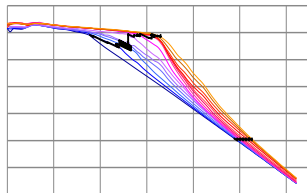
Suspended load (SL)

Bed load (BL)

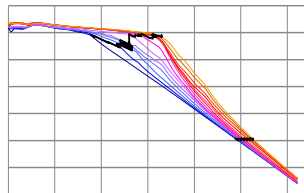
Cohesive sediment (CS)

Non-cohesive sediment (NS)

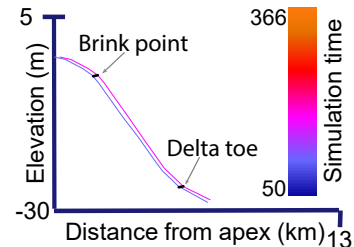
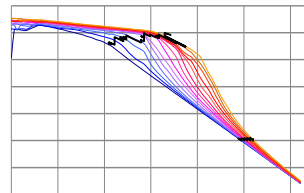
Model 1.1



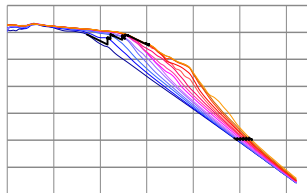
Model 1.2



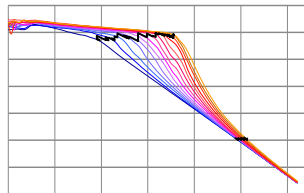
Model 1.3



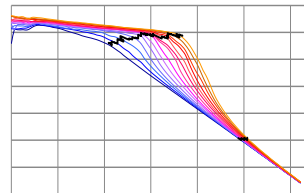
Model 2.1



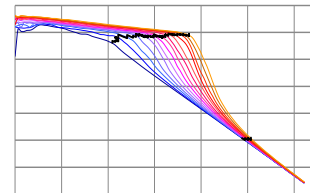
Model 2.2



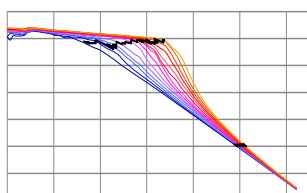
Model 2.3



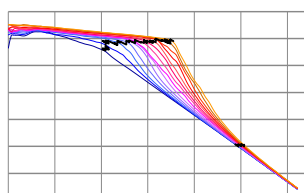
Model 2.4



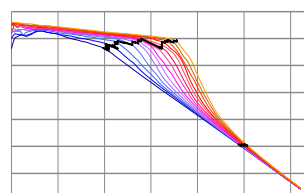
Model 3.1



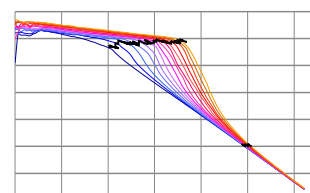
Model 3.2



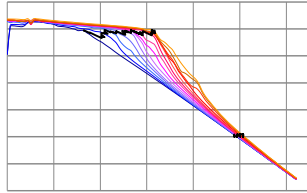
Model 3.3



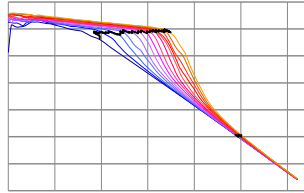
Model 3.4



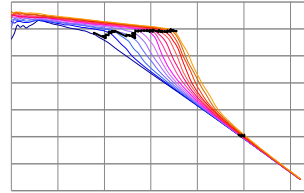
Model 4.1



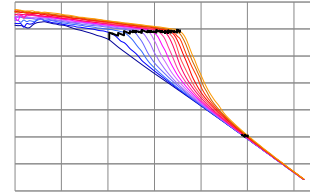
Model 4.2

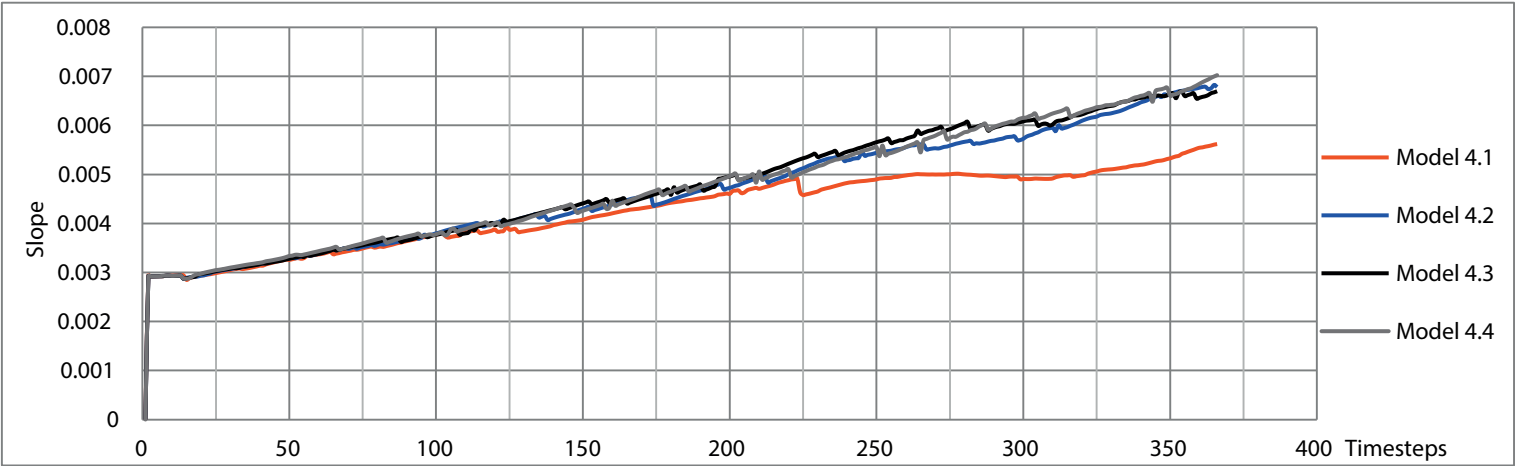
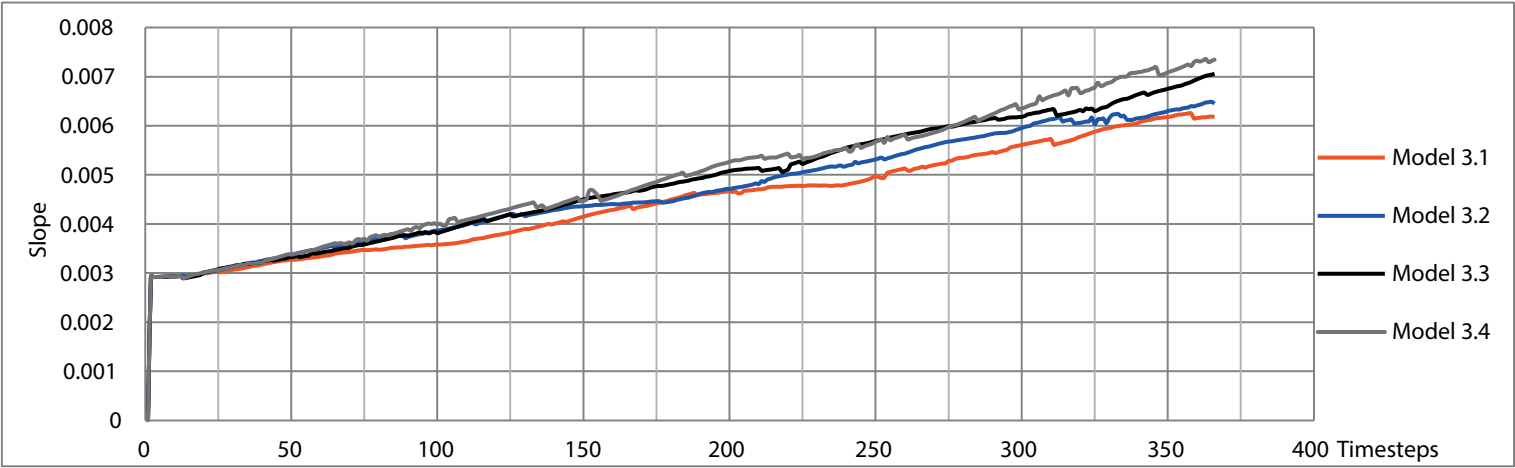
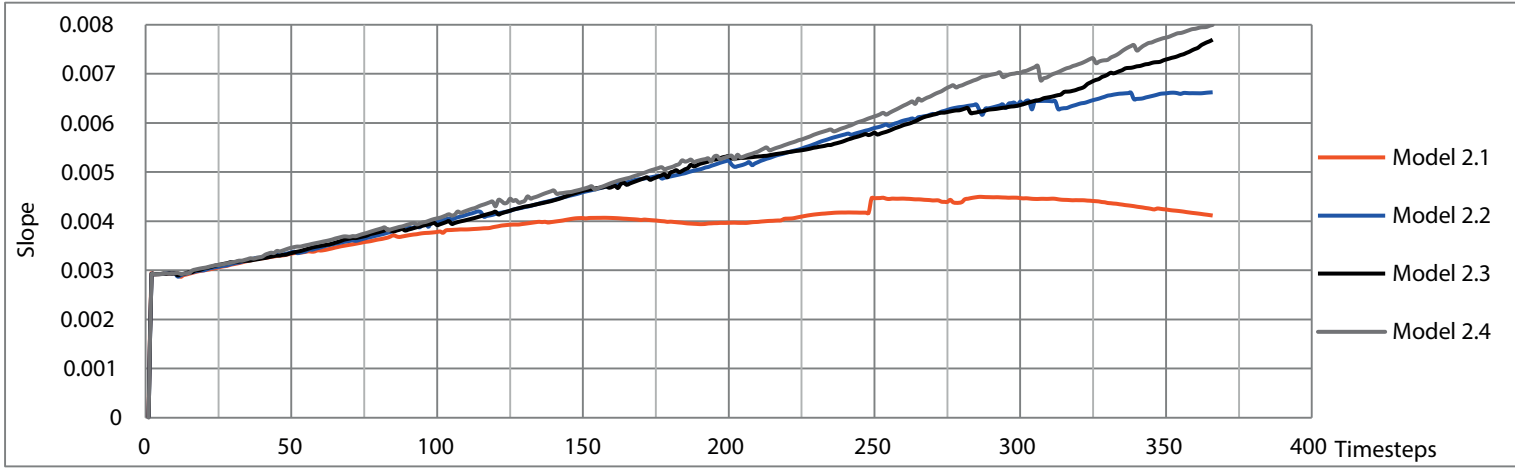
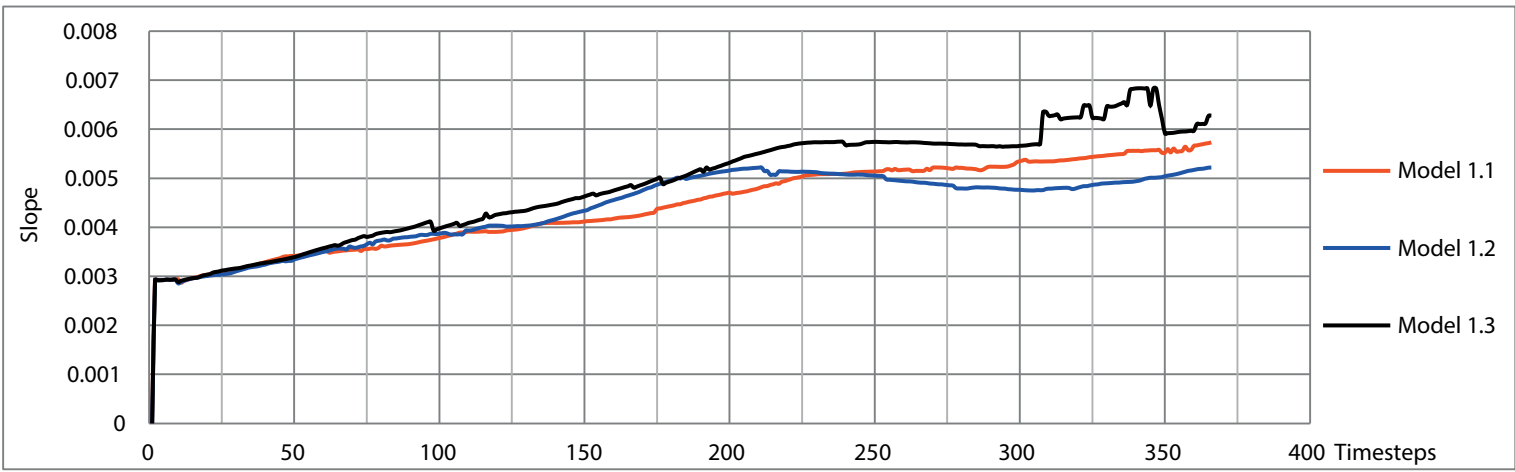


Model 4.3

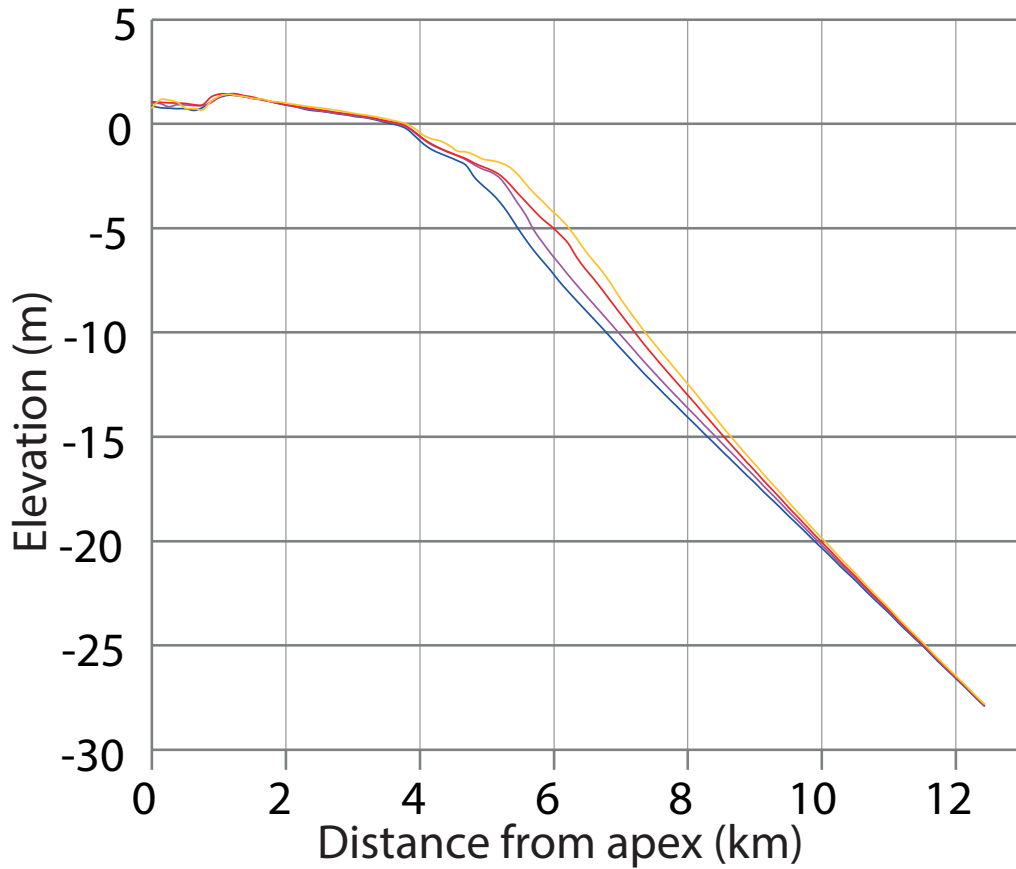


Model 4.4



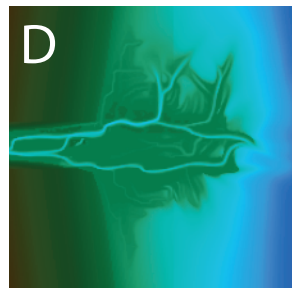
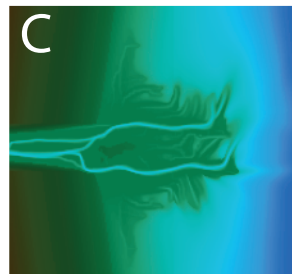
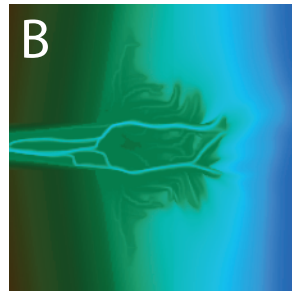
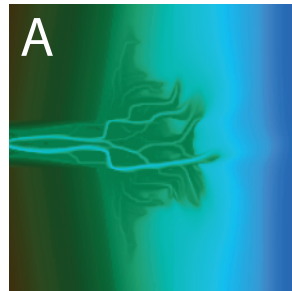
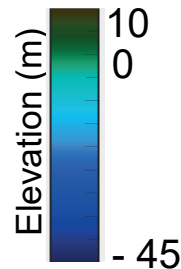


Model 1.1



- (A) Time step 50
- (B) Time step 75
- (C) Time step 100
- (D) Time step 125

10 km



	Non-Cohesive 1 (kg m ⁻³)	Non-Cohesive 2 (kg m ⁻³)	Cohesive 1 (kg m ⁻³)	Cohesive 2 (kg m ⁻³)	Cohesive sediment (%)	Overall bedload (%)	Overall D ₅₀ value (μm)
Model 1.1	0.018	0.042	0.098	0.042	70	5	76
Model 1.2	0.018	0.042	0.098	0.042	70	15	76
Model 1.3	0.018	0.042	0.098	0.042	70	25	76
Model 2.1	0.024	0.056	0.084	0.036	60	5	84
Model 2.2	0.024	0.056	0.084	0.036	60	15	84
Model 2.3	0.024	0.056	0.084	0.036	60	25	84
Model 2.4	0.024	0.056	0.084	0.036	60	35	84
Model 3.1	0.03	0.07	0.07	0.03	50	5	92
Model 3.2	0.03	0.07	0.07	0.03	50	15	92
Model 3.3	0.03	0.07	0.07	0.03	50	25	92
Model 3.4	0.03	0.07	0.07	0.03	50	35	92
Model 4.1	0.036	0.084	0.056	0.024	40	5	99
Model 4.2	0.036	0.084	0.056	0.024	40	15	99
Model 4.3	0.036	0.084	0.056	0.024	40	25	99
Model 4.4	0.036	0.084	0.056	0.024	40	35	99

	Vertical displacement at 2 km from the delta apex (m)	Horizontal brink point displacement (m)	Horizontal delta toe displacement (m)
Model 1.1	2.14	2535	1.74
Model 1.2	2.26	2409	2.08
Model 1.3	2.88	2789	1.74
Model 2.1	1.96	1902	2.08
Model 2.2	2.55	3042	1.39
Model 2.3	3.07	3296	1.04
Model 2.4	3.24	3423	1.04
Model 3.1	2.37	2535	1.39
Model 3.2	2.80	3042	1.04
Model 3.3	3.01	3042	1.04
Model 3.4	3.29	3296	1.04
Model 4.1	2.40	2155	1.04
Model 4.2	3.04	2916	0.69
Model 4.3	3.14	3042	0.69
Model 4.4	3.56	3042	0.69
